MET O 11 TECHNICAL NOTE NO 219

THREE DIMENSIONAL VORTEX METHODS AND THEIR APPLICATION TO THE DIRECT SIMULATION OF TURBULENCE

by

S.P. BALLARD

Met O 11 (Forecasting Research Branch)
Meteorological Office
London Road
Bracknell
Berkshire
England.

OCTOBER 1985

This paper has been submitted to the Journal of Computational Physics.

ABSTRACT

The three dimensional vortex methods of Chorin and Beale and Majda are compared for simple initial data and the similarity of the methods is illustrated. Tests performed using Chorin's method show that the solution is only weakly dependent on most of the adjustable parameters. However there is a strong dependence on the form of the smoothing function required for the velocity integral. The solutions illustrate the rapid stretching of vorticity in inviscid flow but cannot prove conclusively the presence of a singularity in finite time. An important result of this study is that pairing of opposite signed vorticity may be responsible for a significant part of the increase in vorticity and may be a useful concept when parametrizing the effects of viscosity.

1980 Supplemented Mathematical Subject Classification 65M99, 76C05, 76F99.

1. INTRODUCTION

Vortex methods, as described in [1, 2], are a potentially useful tool to use in the attempt to simulate three dimensional turbulence. Computational points can be concentrated in the turbulent, vorticity containing regions of incompressible flow at high Reynolds numbers, thus allowing the resolution of smaller scales of motion than is possible in Eurlerian finite difference or spectral models.

However, it is important to understand the accuracy and limitations of the various methods available for this task. Chorin in [3, 4] used the evolution of the configuration of single computational vortex filaments to study the inertial range of turbulence and produced important conclusions on the intermittency, spectra and singularities in developed turbulence. Thus it is important to verify whether these are properties of turbulence or just of the approximate solutions resulting from this method.

This paper addresses the problem of verifying the consistency of Chorin's method and the accuracy of the solutions obtained as approximations to the solutions of Euler's equations. Thus the evolution of a periodic vortex lattice is computed and the dependence of the solution on various adjustable parameters is studied, extending Chorin's tests in [4]. Comparisons are made with solutions given by an implementation of the discrete method described by Beale and Majda [5] which illustrate the similarity of the methods [6]. The two vortex methods are described in sections 2.3 and 2.4 and the problems associated with the necessity to smooth the integral defining the

velocity field are discussed in section 2.5. The numerical methods and form of the initial data are described in section 3 and the results are given in section 4.

If, as considered, by Chorin [4] the Euler equations can be considered as the high Reynolds number limit of the Navier Stokes equations and the vortex method accurately approximates the Euler equations, we can use the results to investigate the behaviour of turbulent flows. A careful choice of initial data, such as the periodic vortex lattice, will result in self-induced vortex stretching and increasingly chaotic flow with the cascade of energy to diminishing scales. In fact in the absence of viscosity there are suggestions that the vorticity becomes singular in finite time for all but special initial data.

The results of the simulations by Chorin [3, 4] indicate that the L_1 and L_2 norms of vorticity are tending to become infinite in finite time. Work by Morf, Orszag and Frisch [7] and Brachet et al [8], on the Taylor-Green vortex also suggest the possibility of a singularity. However the latter work [8], extending the earlier power series method [7] to higher accuracy and including a comparison with a direct simulation, concludes that the results do not yet provide convincing evidence of the presence of a singularity. Comparisons of results for viscous and inviscid flow indicate that some of Chorin's results may be consistent with the presence of some viscosity in his method.

In section 4.5 we consider the evolution of the $\underline{L}_1$ and $\underline{L}_2$ norms of vorticity in order to investigate the presence of singular solutions to Euler's Equations. In section 4.3 we investigate the properties of the flow and identify a mechanism that becomes important in the rapid

stretching of vorticity whilst conserving the energy of the flow. This dipole pairing of vorticity may be a useful concept when parametrizing the effects of viscosity on the flow.

2. VORTEX METHODS

2.1 Theoretical Background

The Euler equations for three dimensional, incompressible, inviscid flow are

$$\frac{d\vec{\omega}}{dt} = \frac{\partial\vec{\omega}}{\partial t} + (\vec{u}.\nabla)\vec{\omega} = (\vec{\omega}.\nabla)\vec{u} \qquad (1)$$

where $$\vec{\omega} = \nabla x \vec{u} \qquad (2)$$

$$\nabla.\vec{u} = 0 \qquad (3)$$

and $\vec{u}$ and $\vec{\omega}$ are the velocity and vorticity vectors respectively. The combination of (2) and (3) gives the Poisson equation

$$\nabla^2\vec{u} = -\nabla \times \vec{\omega} \qquad (4)$$

If the normal components of velocity on the boundaries are zero the solution to (4) may be written as the Biot-Savart integral

$$\vec{u}(\vec{x},t) = -\frac{1}{4\pi}\int \frac{(\vec{x}-\vec{x}')\times\vec{\omega}(\vec{x}',t)\,d\vec{x}'}{|\vec{x}-\vec{x}'|^3} \qquad (5)$$

Hence the fluid velocity is uniquely determined kinematically from the vorticity field and it is known that the inviscid motion of the vorticity field is given by the local fluid velocity from the theorems of Helmholtz and Kelvin.

2.2 Implementations

In general, vortex methods approximate the vorticity of a fluid by collections of 'vortex elements' such as point vortices or sheets in 2 dimensions, and line vortices, tiles or line segments in 3 dimensions [1, 2]. Their movements are then followed in order to study the behaviour of the flow. The high velocities induced in the flow by these singular distributions of vorticity must be suppressed by applying some type of smoothing to the velocity integral, see section 2.5. This allows stable solutions of the equations of motion by distorting the close interaction of the elements.

Three types of three dimensional vortex methods have been proposed and used for various calculations [2]. These can be described as firstly the thin filament approximation, secondly bundles or distributions of computational filaments and finally the discrete or 'arrow' methods.

The thin filament approximation [9, 10] uses single line vortices of zero cross-sectional area and constant circulation, Γ, to study the behaviour of isolated tubes of vorticity such as in aircraft trailing vortices and vortex rings. If the tube has finite core of cross-sectional radius σ and area $\underline{A}$

$$\Gamma = \int_{\underline{A}} \vec{\omega} \cdot d\vec{A} \qquad (6)$$

In order to study smooth or distributed fields of vorticity the other two methods are invoked. The first considers the vorticity field to be given by a sum over a collection of line vortices [11, 3, 4]. The final group of methods can be referred to as Lagrangian grid point methods. The vorticity is defined at points on an initial grid [5] or

defined as vortex segments or sticks [12, 13] with no assumed connection, in contrast to the whole filament approximations of the first two groups. The vortex element locations are moved with the local smoothed velocity and the vorticity vector is updated at each step using Eq. (1).

In this paper direct comparisons are made between a method of the second category, Chorin's method, and a discrete Lagrangian grid point method, Beale and Majda's method.

2.3 Chorin's Method

Chorin [3, 4] supposes that the initial data can be approximated by a collection of $\underline{M}$ vortex tubes of small but finite cross-sections $\underline{A}$. The circulations, $\Gamma_{\underline{i}}$, of these tubes are constants of the motion given by Eq. (6) so that the velocity integral reduces to one along computational filaments or line vortices.

$$\vec{u}(\vec{x},\underline{t}) = -\frac{1}{4\pi} \sum_{\underline{i}=1}^{\underline{M}} \Gamma_{\underline{i}} \int \left(\frac{g(\underline{a}/\delta)\,\vec{a}}{\underline{a}^3} \right) \times \frac{\partial \vec{r}_{\underline{i}}(\underline{s})}{\partial \underline{s}}\, d\underline{s} \qquad (7)$$

where $\underline{s}$ is the distance along the filament,

$\vec{r}_{\underline{i}}(\underline{s})$ is the location of the filament

$\vec{u}(\vec{x},\underline{t})$ is the velocity field at position $\vec{x}$ at time $\underline{t}$

and $\vec{a} = \vec{x} - \vec{r}_{\underline{i}}(\underline{s})$, $\underline{a} = |\vec{a}|$

The smoothing function $\underline{g}(\underline{a}/\delta)$ removes the singularity of the velocity integral by taking account of the finite cross-section of the vortex tubes and so avoids the infinite velocity induced by close neighbour interaction on infinitely thin filaments.

Chorin [3] used

$$g(a/\delta) = \begin{cases} 1 & \text{if } a \geq \delta \\ a^2/\delta^2 & \text{if } a < \delta \end{cases} \qquad (8)$$

The filaments are further approximated by line segments and the motions of the end points of the segments, or nodes, are followed. Vortex stretching is represented by the increase in separation of adjacent nodes, that is the increase in length of the vortex segments. Thus the velocity integral is approximated by the sum of contributions due to line segments with the separation, a, calculated at the midpoint of the segment (the rectangular rule).

The lengths of the segments are limited to a maximum value of λ_m and once this value is exceeded the segments are split at their midpoints. Therefore the number of nodes increases as the length of the filaments, and hence vorticity, increases.

Thus for the node $\vec{x}_{m}^{n}$ at the start of segment n on filament m

$$\frac{\partial \vec{x}_m^n(t)}{\partial t} = \vec{u}(\vec{x}_m^n(t)) \qquad (9)$$

$$\vec{u}(\vec{x}_m^n(t)) = -\frac{1}{4\pi} \sum_{i=1}^{M} \Gamma_i \sum_{j=1}^{N_i} \frac{g(a/\delta)\, \vec{a}_i^{\,j}{}_m^n \times \Delta\vec{s}_i^{\,j}}{a^3} \qquad (10)$$

where $m = 1, M$, $n = 1, N_m$

$$\vec{a}_i^{\,j}{}_m^n = \frac{1}{2}(\vec{x}_i^{\,j'} + \vec{x}_i^{\,j}) - \vec{x}_m^n \quad , \qquad j' = (j+1) \bmod(N_i)$$

$$a = |\vec{a}_i^{\,j}{}_m^n|$$

$$\Delta\vec{s}_i^{\,j} = \vec{x}_i^{\,j'} - \vec{x}_i^{\,j}$$

The solution may thus depend on a variety of parameters such as the number of filaments, the number of segments per filament, the cutoff distance δ and λ_m as well as the function $g(a/\delta)$, the time integration scheme and method of integrating along a segment.

Recently Greengard [14] has produced a convergence theorem for filament methods of this type by reformulating them into a version of the discrete methods, described by Beale and Majda [5], in a curved coordinate system. This proof assumes smooth initial data and that the time step, separation of node points and the width of the smoothing function, related to δ, are all sufficiently small. The separation of the node points must also be sufficiently smaller than the width of the smoothing function and the proof applies for a finite interval of time.

2.4 Beale and Majda's Method

In the algorithms described by Beale and Majda [5, 15] the velocity is updated crudely as in Chorin's method. However the vortex stretching is now incorporated via a Lagrangian update. The trajectory of a fluid particle starting at time zero at the position is again determined by the equation

$$\frac{\partial \vec{x}_\alpha(t)}{\partial t} = \vec{u}(\vec{x}_\alpha(t)) \quad , \quad \vec{x}_\alpha(0) = \vec{\alpha} \qquad (11)$$

$$\vec{\alpha} = (\alpha_1, \alpha_2, \alpha_3)$$

where the velocity $\vec{u}$ is given by an equation of the form of Eq. (5). The stretching of the vorticity is described by the vorticity equation (1). This can be expressed in a Lagrangian formula, [5, 16]

$$\frac{d\vec{\omega}(\vec{x}_\alpha(t))}{dt} = \vec{\omega}(\vec{x}_\alpha(0)) \cdot \nabla_\alpha \vec{u}(\vec{x}_\alpha(t)) \qquad (12)$$

involving the gradients of velocity at time t with respect to the initial position of the points $\vec{x}_\alpha(t)$ where $\nabla_\alpha \vec{u}(\vec{x}_\alpha(t))$ is the 3 x 3 Jacobian matrix

$$\frac{\partial \vec{u}_i(\vec{x}_\alpha(t))}{\partial \alpha_j} \qquad 1 \leq i,j \leq 3 \tag{13}$$

and $\vec{\omega}(\vec{x}_\alpha(0))$ is the initial vorticity of the fluid particle starting at position $\vec{\alpha}$.

The initial vorticity fields are discretized onto a three dimensional uniform grid of gridstep h. Values of position, velocity and vorticity are held on the grid, the grid data points moving with the fluid but the velocity derivatives being calculated with respect to their initial positions. This minimizes errors due to errors in evolving quantities.

There are thus two coupled nonlinear ordinary differential equations for the vorticity and positions of fluid initially at the grid points $\vec{x}_i(0) = (lh, mh, nh) = \vec{\alpha}_i$

$$\frac{\partial \vec{x}_i(t)}{\partial t} = \vec{u}_i^h(t)$$

$$\frac{d\vec{\omega}_i(t)}{dt} = \nabla_\alpha \vec{u}_i^h(t) \cdot \vec{\omega}_i(0), \quad \vec{\omega}_i(0) = \vec{\omega}(\vec{x}_i(0)) \tag{14}$$

Since for $\vec{\omega}_i(0) = 0$, $\frac{d\vec{\omega}_i(t)}{dt} = 0$ data need only be held on a set of points $i=1,N$ slightly larger than the set of points falling in the support of the initial vorticity field. The method follows the motion of these grid points, referred to as nodes, and the evolution of their

associated vorticity. $\vec{u}_i^h(t)$ again represents a smoothed velocity integral so that

$$\vec{u}_i^h(t) = -\frac{1}{4\pi} \sum_{j=1}^{N} \frac{[\, g(a/\delta)\, \vec{a} \times \vec{\omega}_j(t)]\, h^3}{a^3} \qquad (15)$$

where $\vec{a} = \vec{x}_i(t) - \vec{x}_j(t)$, $a = |\vec{a}|$, $i = 1, N$

No provision is made to increase the number of vortex elements as their separation increases in this implementation. Therefore as stretching occurs and separation increases there is a loss of accuracy. However as the aim of the study here is to compare solutions obtained with different resolution remeshing was not used.

Beale and Majda (5) have proved that methods of this type are stable and convergent with arbitrarily high accuracy for a period of time T. The stability and accuracy depends on the smoothing or cut off function g(a), the difference operator ∇_α^h and the choice of the parameter δ and the initial grid size h.

Recently Anderson and Greengard [6] have pointed out that the two methods of Chorin and Beale and Majda are essentially the same as in fact the vortex stretching in Chorin's method is carried out using a forward finite difference operator applied to the velocity fields with respect to the initial configuration of the vortices. The work reported here illustrates this point.

However the two methods can obviously be used in different situations, Beale and Madja's method being more applicable to distributed fields than is Chorin's method.

2.5 Smoothing of the velocity Integral

In order to calculate the discretized velocity integral the singularity must be removed by a method that accurately approximates the exact velocity field. There have been various different approaches. Either the vortex elements are considered to have finite cores or associated non-singular distributions of vorticity [11]. Then the elements are often referred to as vortex blobs. Alternatively a short interval, or volume, is removed from the velocity integral [17] or the singular integral is just assumed to be replaced by an accurate smooth approximation [5].

These methods can all be considered to include some type of smoothing function $\underline{g}(\underline{a}/\delta)$, with associated parameter δ in the velocity integral as in Eq (7) and Eq (15). Anderson and Greengard [6] have shown that smoothing of the velocity integral by a function $\underline{g}(\underline{a}/\delta)$ is equivalent to approximating the vorticity field by a collection of vortex blobs.

They consider the velocity field $\vec{u}$ to be the convolution of a kernel $\vec{K}$ with the vorticity field $\vec{\omega}$ expressed as

$$\vec{u} = \vec{K} * \vec{\omega} \tag{16}$$

where $\vec{K} = -\frac{1}{4\pi}\frac{\vec{a}\times}{\underline{a}^3}$, $\vec{a} = \vec{x}-\vec{x}'$, $\underline{a} = |\vec{a}|$

If the singular kernel $\vec{K}$ is convolved with $\psi_\delta(\underline{a})$, a smooth approximation to the Dirac delta function of width δ Eq. (16) is replaced by

$$\vec{u}_\delta = \vec{K}_\delta * \vec{\omega} \tag{17}$$

where $\vec{K}_\delta = \vec{K} * \psi_\delta(\underline{a})$

Then $g(a/\delta)$ is defined by Eq. (18)

$$\vec{K}_\delta = \vec{K} \; \underline{g}(\underline{a}/\delta) \tag{18}$$

and $$\psi_\delta(\underline{a}) = \frac{\psi(\underline{a}/\delta)}{\delta^3} \tag{19}$$

where $\int \psi(x) \, d\vec{x} = 1$

Eq. (17) can be considered as

$$\vec{u}_\delta = \vec{K} * \vec{\omega}_\delta \tag{20}$$

and $$\vec{\omega}_\delta = \psi_\delta(\underline{a}) * \vec{\omega} \tag{21}$$

where $\vec{\omega}_\delta$ is a vorticity field smoothed by $\psi_\delta(\underline{a})$, equivalent to a collection of vortex blobs, so that $\vec{u}_\delta$ is the exact field due to the vortex blobs.

In the thin filament approximation the form of the function $\underline{g}(\underline{a}/\delta)$, and hence $\psi_\delta(\underline{a})$, and the value of δ are usually chosen to carefully match the calculated velocity with that due to, for example, vortex rings with given core sizes and vorticity distributions. The parameter δ is then related to the core radius σ [9, 17]. These methods attempt to take account of the core dynamics that cannot be treated explicitly. However they are accurate only if $\sigma/\underline{R} \ll 1$ [10, 18], where $\underline{R}$ is the radius of curvature of the filament, so that short wavelength disturbances, and possibly close interactions, are mistreated.

In the discrete methods used in the convergence proofs [5, 6, 19] ψ and δ are determined by the need to provide stability and accuracy whilst avoiding infinite induced velocities rather than a need to account for core dynamics. The proofs assume that sufficient resolution

of the vorticity field, particularly in the core, has already been obtained and δ is closely related to the original mesh spacing $\underline{h}$. The accuracy of these vortex methods are controlled by the choice of ψ and the relative sizes of δ and $\underline{h}$. Beale and Majda [5] require δ to be sufficiently larger than $\underline{h}$ and establish the relationship $\delta = \underline{h}^{\underline{q}}$, $0 \leq \underline{q} \leq 1$ in order to balance errors in smoothing and discretization which are opposite in character. Smoothing errors are worse for large δ and discretization errors are improved by increasing δ. Accuracy can be improved by using higher order accurate ψ [5, 6].

However it is not clear what should determine the choice of smoothing function and the parameter δ in the limit of low resolution when only a single or few elements are used in the cross-section as in Chorin's work [3, 4]. Should the smoothing represent properties of a given distribution of vorticity in the core of a vortex filament or just be a means of stabilizing the method that allows convergence as the number of the filaments increases?

It is not obvious what flow is being modelled when Chorin [3, 4] follows the evolution of the configuration of single vortex filaments with the form of $\underline{g}(\underline{a}/\delta)$ given by Eq. (8), δ being kept constant in time. It can be argued that it is the case of single line vortices with zero cross-sectional area, where $\underline{g}(\underline{a}/\delta)$ just produces stability and removes the singularity. Alternatively a vorticity field composed of elements with small support, determined by δ, ie vortex blobs or an approximation to a general flow containing more widespread vorticity are being studied. Obviously it is important to understand the relationship

between the solution obtained using the smoothed velocity integral at low resolution and the solution of the Euler equations if the results are to be interpreted in terms of the properties of turbulent flow.

Recently Greengard [14], using a method very similar to Chorin's, has studied the behaviour of solutions of the smoothed equations, which he calls the E_δ equations, using both single filaments and bundles of filaments. The E_δ equations converge to the solutions of Euler's equations as δ tends to zero [5, 6, 14] as long as the separation of the vortex elements h tends to zero more rapidly and the timesteps also tend to zero.

He assumed, and illustrated, that for a multifilament calculation increasing resolution and reducing timesteps for constant δ will produce a converged solution of the E_δ system. He considered that in the case of single filament calculations the computed solution converges towards a weak solution of the E_δ system as the resolution along the filaments is increased for fixed δ. Thus we need to understand the relationship between these weak solutions of the E_δ system and the solutions of the Euler equations.

The dependence of the solution of the smoothed equations on the smoothing function $\underset{\sim}{g}(\underset{\sim}{a}/\delta)$ is studied in section 4.4.

One further consideration required in single filament calculations is whether or not the parameter δ, which can obviously be related to the core size of a vortex filament, should be kept constant throughout the evolution of the flow in order to correctly approximate the solutions of Euler equations. From conservation of volume, as a vortex tube of finite cross-section stretches its cross-sectional area must decrease. Since the circulation is conserved the vorticity will increase. When δ

is kept constant the strain rate can only increase due to the presence of more vorticity in the fluid. The effect of increased velocities near filaments, due to the production by stretching of intensified vorticity inside a smaller cross-section, is removed. Leonard [11] considers that use of a constant core size or δ acts as a sub grid scale parametrization of viscosity proportional to vortex stretching. Thus smaller scale structure, due to variable amounts of stretching along the filament, may be lost. This problem is also discussed in section 4.4.

3. COMPARISON OF TWO VORTEX METHODS

3.1 Form of Initial Data

Direct comparison of the Beale and Majda method and Chorin's method without the problem of the initial representation of curved vortex filaments is possible by considering the evolution of a periodic lattice of straight filaments. Flow is considered in a unit cube with periodic boundary conditions. Each unit cube contains two filaments crossing at right angles and separated by 0.1 units in the perpendicular $\underline{z}$, or $\underline{x}_3$ direction, see Fig. 1a).

One filament has vorticity parallel to the $\underline{x}$, or $\underline{x}_1$, axis and the other parallel to the $\underline{y}$, or $\underline{x}_2$, axis, each having unit circulation and an assumed radius $\underline{r}_o$.

This is a simple situation in which to study vortex stretching as each filament causes the other to rotate about it producing stretching and compression along their lengths.

The initial data contains symmetry since the initial position vectors of the axes of the filaments, $\vec{X}_A$ and $\vec{X}_B$ are

$$\vec{X}_A = (0.0, \underline{x}_2, -0.05), \quad -0.5 \leq \underline{x}_2 \leq 0.5 \qquad (22)$$

$$\vec{X}_B = (\underline{x}_1, 0.0, 0.05), \quad -0.5 \leq \underline{x}_1 \leq 0.5 \tag{23}$$

In fact at all times the flow at $\underline{x}_3 < 0$ can be obtained from that calculated at $\underline{x}_3 > 0$.

since if $$\vec{u}(\underline{x}_1, \underline{x}_2, \underline{x}_3) = (\underline{u}_1, \underline{u}_2, \underline{u}_3) \tag{24}$$

$$\vec{u}(\underline{x}_2, \underline{x}_1, -\underline{x}_3) = (\underline{u}_2, \underline{u}_1 - \underline{u}_3) \tag{25}$$

Therefore the velocities and positional increments, also vorticity increments in Beale and Majda's method, of only one filament needs to be calculated and they can then be applied to the second filament. This not only reduces the number of calculations required per time step but preserves the symmetry of the flow.

3.2 Boundary Conditions

The flow is considered inside the cube

$$-0.5 \leq \underline{x}_i \leq 0.5 \quad \underline{i} = 1,2,3 \tag{26}$$

with periodic boundary conditions.

The use of periodic boundary conditions allows consideration of conservation of energy in the unit cube. However it is not easy to implement these conditions due to the infinite number of images that should be included. In fact the initial velocity induced on each of the filaments is that due to a 2-D infinite array of perpendicular filaments but this velocity does not appear to be well defined. This can be seen by considering an infinite number of periodic rows. However following Chorin [3,4] and considering that $1/\underline{a}^3$ is small for large $\underline{a}$, we can neglect contributions (to the velocity integrals) from distant vorticity

with a greater than Rmax. Hence if Rmax is less than 0.5 only one 'nearest' vortex element image needs to be considered. A value of Rmax = 0.495 is used.

3.3 Time Integration scheme

A fourth order Runge-Kutta time integration scheme was used to update the positions of the nodes in Chorin's method and the positions and vorticities of the grid points in Beale and Majda's method. An initial timestep of dt = 0.001 was used with an arbitrary test for stability as in Chorin [4].

$$P = dt \times umax < h \qquad \text{Beale and Majda's method} \qquad (27)$$

$$P = dt \times umax < F < \lambda_m \qquad \text{Chorin's method}$$

where umax is the maximum velocity of a node or grid point. The timestep is halved if P exceeds the limit.

3.4 Implementation of Chorin's Method

The two filaments were each represented as single computational line vortices of circulation $\Gamma = 1$. A limiting segment length of $\lambda_m = 0.05$ was used and the lengths of the segments were checked every timestep. F was set at 0.03.

Initially integrations were run starting with each filament split into N equal length segments. However it became obvious (see section 4.1) that better resolution, with fewer points could be obtained by decreasing the initial segment lengths only in the regions where rapid stretching occurred. Hence a posteriori initial segments of unequal lengths, λ_{oi}, were chosen varying from λ_o to $\lambda_o/128$ with $\lambda_o = 0.05$. This initial data is used in the analysis of the evolution of flow.

3.5 Implementation of Beale and Majda's Method

The two crossed vortex filaments were discretized onto a grid of length h. For initial calculations the cross-sections of the filaments were limited to one grid point only and a value of vorticity was assigned to these points so that the circulation was equal to one for all the resolutions used, h = 0.05, 0.025, 0.0125 and 0.003215. Each filament was represented by $N+2$ points along the length where $N=1/h$. Initial vorticities $\vec{\omega}_A(m)$ and $\vec{\omega}_B(m)$ were assigned to points $\vec{X}_A(m)$ on the first filament and $\vec{X}_B(m)$ on the second filament respectively where

$$\vec{X}_A(m) = (0.0,\ x_2(m),\ -nh) \tag{29}$$

$$\vec{X}_B(m) = (x_2(m),\ 0.0,\ nh) \tag{30}$$

with $x_2(m) = (m-2)h$, $m=1,\ N+2$

$n = 0.05/h$

and $\vec{\omega}_A(m) = (0,\ \omega_o,\ 0)$, $\vec{\omega}_B(m) = (\omega_o, 0, 0)$ where $\omega_o = 1/h^2$

No other points were required as initially the direction of the vorticity was constant along each filament.

The derivatives of the velocity required in the vorticity equation are fully derived from the positions of the initial vorticity and approximated by a second order centred difference operator.

3.6 Smoothing Function

The smoothing function $g(a/\delta)$ used in the calculations is defined as

$$\begin{aligned} g(a/\delta) &= 0 && a > Rmax \\ g(a/\delta) &= 1 && \delta < a \leq Rmax \\ g(a/\delta) &= a^3/\delta^3 && a \leq \delta \end{aligned} \tag{31}$$

with $\delta = 0.05$, $Rmax = 0.495$

This corresponds to

$$\psi_\delta = 3/(4\pi\delta^3) \quad \text{for } \underline{a} \leq \delta \tag{32}$$
$$= 0 \quad \text{for } \underline{a} > \delta$$

and a vorticity distribution of

$$|\vec{\omega}(\underline{a})| = \frac{3\,(\delta^2 - \underline{a}^2)^{1/2}}{2\pi\delta^3} \quad \text{for } \underline{a} \leq \delta \tag{33}$$

This is slightly different from the form used by Chorin [3, 4] but allows easier comparison between Beale and Majda's and Chorin's methods.

This smoothing function is discontinuous at $\underline{a} = \delta$ and so does not necessarily have the high order accuracy of these described by Beale and Madja [20]. However calculations to $\underline{t} = 0.2$ using their second order accurate $\underline{g}(\underline{a}/\delta) = \tanh(\underline{a}^3/\delta^3)$ and exponential form $\underline{g}(\underline{a}/\delta) = 1 - \exp(-\underline{a}^3/\delta^3)$ with $\delta = 0.05$ gave very similar results to the form used here.

3.7 Diagnostics

The principal diagnostics calculated are the L_1 and L_2 norms of vorticity defined as

$$\underline{L}_1(\omega) = \int |\vec{\omega}| \, \underline{dV} \tag{34}$$

$$\underline{L}_2(\omega) = \int |\vec{\omega}|^2 \underline{dV} \tag{35}$$

These are simply calculated in Beale and Majda's method as

$$\underline{L}_1^{\underline{h}}(\omega) = \sum_{\underline{m}} |\vec{\omega}_A(\underline{m})| \, \underline{h}^3 + \sum_{\underline{m}} |\vec{\omega}_B(\underline{m})| \, \underline{h}^3 \tag{36}$$

$$\underline{L}_2^{\underline{h}}(\omega) = \sum_{\underline{m}} |\vec{\omega}_A(\underline{m})|^2 \underline{h}^3 + \sum_{\underline{m}} |\vec{\omega}_B(\underline{m})|^2 \underline{h}^3 \tag{37}$$

In Chorin's method the L_1 norm of vorticity is given by the total lengths of the filaments in the unit cube.

$$L_1{}^c(\omega) = \sum_{i=1}^{M} \sum_{j=1}^{N_i} \lambda_i{}^j \tag{38}$$

where $\lambda_i{}^j$ is the length of a segment. Similarly, if we assume that the radial distribution of vorticity remains constant as the vortex filaments stretch, the L_2 norm is given by

$$L_2{}^c(\omega) \propto \sum_{i=1}^{M} \sum_{j=1}^{N_i} \frac{(\lambda_i{}^j)^2}{V_i{}^j} \tag{39}$$

where $V_i{}^j$ is the volume associated with the segment.
Thus we need the extra variable $V_i{}^j$ which remains constant unless the segments are split. Then the value must be halved and assigned to each half segment. Initially

$$V_i{}^j = \pi r_o{}^2 \lambda_{oi}{}^j \tag{40}$$

where r_o = initial radius of filament

$\lambda_{oi}{}^j$ = initial length of segment j on filament i

This extra variable also enables us to keep track of the amount of stretching that a single segment has undergone during the evolution of the flow. So that the amount of stretching $S_i{}^j$ is given by

$$S_i{}^j = \lambda_i{}^j/\lambda_{oi}{}^j = \lambda_i{}^j \pi r_o{}^2/V_i{}^j \tag{41}$$

The method of assigning vorticity to the grid points in Beale and Majda's method means that the definitions of circulation and L_1 norm of vorticity are directly comparable between Chorin's method and Beale and Majda's method. However the L_2 norms differ by factors depending on the resolution h in Beale and Majda's method. So that $L_2{}^c(\omega)$ should be compared with $h^2 L_2{}^h(\omega)/\pi r_o{}^2$.

For periodic boundary conditions we can consider the ability of the methods to conserve energy in a unit cube. The total kinetic energy per unit cube was approximated by using the velocities calculated on a 20 x 20 x 20 grid. It should be possible to calculate the energy directly from the vorticity distribution but it is not easy to find a method consistent with the use of the smoothing function. Tests with 40^3 and 80^3 grids indicate that the 20^3 grid approximation is reasonable.

4. RESULTS OF NUMERICAL INTEGRATIONS

4.1 Chorin's Method

The standard integration, as described in section 3.4 used the smoothing function of section 3.6 and a fourth order Runge-Kutta time-integration scheme. The various adjustable parameters were set so that $\delta = 0.05$, $Rmax = 0.495$, $\lambda_m = 0.05$, $F = 0.03$, and timestep $dt = 0.001$. The initial data had maximum resolution in regions of maximum stretching as determined by previous trial runs, so that the λ_{oi} were unequal.

The initial configuration of the vortex filaments in a unit cube is shown in the top row of Fig. 1 in plan and side views and a three dimensional projection. The symbols mark the original node points. The two filaments become increasingly tangled, as each induces the other to move around it and the evolution is shown in the rest of Fig. 1.

After a slow initial increase in vorticity, until about $t = 0.2$, there was then a rapid increase in both the L_1 and L_2 norms of vorticity. $L_1(\omega)$ had only increased by approximately 50% at $t = 0.2$ but was over thirty times its initial value when the integrations were

stopped at $\underline{t}$ = 0.399. The integrations were stopped when each filament had 999 segments produced from the 160 initial segments. The evolution of $\underline{L}_1(\omega)$ is shown in Fig. 2 and Table I.

One test of the stability of the method is the conservation of kinetic energy and as seen from table II this is roughly achieved.

In order to study the accuracy of the solution obtained by Chorin's method its dependence on the spatial resolution, boundary conditions, temporal resolution and time integration schemes was investigated.

The spatial resolution of the method is determined by the initial segment lengths $\lambda_{o\underline{i}\underline{j}}$ and the maximum segment length $\lambda_{\underline{m}}$.

Integrations with $\lambda_{\underline{m}}$ = 0.05 and all $\lambda_{o\underline{i}\underline{j}}$ = 0.05, 0.025 or 0.0125 each produced the same general evolution but with greater resolution of the curvature as $\lambda_{o\underline{i}\underline{j}}$ decreased and hence better accuracy at later times. It became obvious that the extra resolution was not required where little stretching occurred and so variable segment lengths were used in the standard integration. Table I shows that the evolution of $\underline{L}_1(\omega)$ for equal $\lambda_{o\underline{i}\underline{j}}$ = 0.05 agrees well with the standard case until $\underline{t}$ = 0.3. At later times the configuration, $\underline{L}_1(\omega)$ and $\underline{L}_2(\omega)$ diverge slightly for the two cases due to increasing errors resulting from lack of resolution when $\lambda_{o\underline{i}\underline{j}}$ = 0.05.

With $\lambda_{o\underline{i}\underline{j}}$ as in the standard integration, test runs to $\underline{t}$ = 0.3 show reproducibility of the solution as $\lambda_{\underline{m}}$ was decreased from 0.05 to 0.025 and 0.0125, providing extra resolution of curvature. The configurations were slightly smoother at higher resolution but the similarity of the solutions does not justify the extra computational expense, see table I. There were 757 segments per filament at $\underline{t}$ = 0.3 for $\lambda_{\underline{m}}$ = 0.0125 as opposed to 228 for $\lambda_{\underline{m}}$ = 0.05 and only a 5% difference in $\underline{L}_1(\omega)$.

Thus the spatial resolution of the standard integration can be considered to be sufficient during the period of comparison. The kinetic energy was roughly conserved in all the comparison integrations.

In order to test the sensitivity of the results to the approxiation to periodicity the maximum separation of points included in the calculation of velocity was increased to 0.995 from 0.495. This means that more 'images' are included in the calculation and as Rmax tends to infinity the solution will tend to the correct solution for periodic data. The results are very similar to those from the standard case as shown in table I. A run to t = 0.2 with no limit Rmax but including only the 27 nearest images of a segment also showed close agreement, see Table I. This justifies a posteriori the neglect of contributions from distances greater than Rmax = 0.495. Again kinetic energy was roughly conserved.

The temporal resolution of the method is determined by the initial timestep, dt, and the parameter F. With dt = 0.001, as in the standard integration, and initial umax = 1.56 a maximum displacement per timestep of 19 times the initial displacement is allowed by the value F = 0.03. In order to limit the allowed displacement to closer to its initial value an integration to t = 0.3 was performed using F = 0.002. This showed no difference from the solution obtained with the higher value of F, see table I, even though the timestep had been reduced to dt = 0.00025. Thus the standard integration had not lost any temporal resolution as the flow evolved.

In order to try to decrease the CPU time required for the integrations simpler time-integration schemes were tried, such as centred difference and Euler forward difference. All schemes agreed well until approximately $\underline{t}$ = 0.2 as shown in Table II.

Time splitting occurred in the centred differencing scheme solution which became evident as an oscillation in the maximum node point velocity by $\underline{t}$ = 0.274 and an increase in kinetic energy of greater than 100% by $\underline{t}$ = 0.36. The stability was improved by using a time filter such that

$$\vec{x}^{\underline{n}+1} = (1-\zeta)\,(\vec{x}^{\underline{n}-1} + 2.\underline{dt}.\vec{u}(\vec{x}^{\underline{n}})) + \zeta(2\vec{x}^{\underline{n}} - \vec{x}^{\underline{n}-1}) \qquad (42)$$

where $\underline{n}$ indicates the time level and ζ is a weighting factor. Using ζ = 0.1 good agreement is then found with the fourth order Runge-Kutta solution.

The Euler first order forward difference time integration scheme, as used by Chorin [4] diverges from the standard solution after $\underline{t}$ = 0.2 by which time the kinetic energy is also increasing, indicating that the solution cannot be trusted.

Thus the solution was independent of the time integration scheme until about $\underline{t}$ = 0.2. At later times the Euler scheme loses accuracy and diverges from the solution obtained from the higher order schemes.

4.2 Beale and Majda's method

As the resolution along the filaments is increased the configuration of the filaments appears to be converging to that produced by Chorin's method as can be seen from Fig 3. However the resolution is unable to cope with the rapid increase in vorticity after about t = 0.2 and the solutions diverge as can be seen from table III and Fig 2. The

solutions are able to follow the solution from the standard integration of Chorin's method for longer periods into the integration as the resolution is increased. The case with $\underline{h}$ = 0.003125 almost matching the standard integration out to $\underline{t}$ = 0.25, compare Fig 4, Fig 1c) and d). $\underline{L}_1(\omega)$ shows a smaller increase by $\underline{t}$ = 0.4 than with Chorin's method although the increase in $\underline{L}_1(\omega)$ with resolution seems to indicate that the solutions are converging to that obtained by Chorin's method. Obviously remeshing is required to compute accurate solutions once rapid stretching has occurred. The solutions lose accuracy after $\underline{t}$ = 0.2 to $\underline{t}$ = 0.25 depending on the initial resolution and the kinetic energy increases with time indicating instability.

These results provide evidence to support the accuracy of the solution obtained by Chorin's method and show the similarity between the two types of methods.

4.3 Description of Flow

We see from section 4.1 that the solution obtained from Chorin's method for the given smoothing function is reproducible and only weakly dependent on the spatial and temporal resolution, boundary conditions and time integration scheme. Also its accuracy is supported by the solution obtained from the Beale and Majda method once it has sufficient spatial resolution. Therefore we can consider with confidence the features of the predicted flow as the converged solution for the given smoothing function.

As mentioned in section 4.1 the vorticity of the fluid as measured by $\underline{L}_1(\omega)$ and $\underline{L}_2(\omega)$ increased gradually until $\underline{t}$ = 0.2 and then rapidly until the end of the integration at $\underline{t}$ = 0.399. There was only an increase of 50% in $\underline{L}_1(\omega)$ by $\underline{t}$ = 0.2 and then a twenty fold increase in

the next interval of $\Delta\underline{t} = 0.2$. However despite this rapid increase in vorticity the kinetic energy of the flow is apparently conserved. Chorin [4] noted that the constraint of energy conservation prevented even spreading of the vorticity and that stretched filaments are forced into tangles or folds so that their associated velocity fields cancel. In this case close alignment of opposite signed vorticity is evident as well as some tangling. This is illustrated in Fig 5. By $\underline{t} = 0.3$ about 73% of the length of each filament is aligned within a distance δ of another section, of either the same filament or the other filament, so that their vorticity vectors are in opposite directions, the angles between the vorticity vectors being greater than 160°. 40% is within 0.02 and the pairs get closer together as time increases. These dipole sections will have only a small net effect on the velocity field away from their locations and energy is conserved despite the greatly increased vorticity present in the flow.

This vortex dipoling may be responsible for the rapid increase in the vorticity. A pair of rectilinear line vortices will induce motion on each other such that they will move in a direction normal to the line joining their axes and hence sections of paired filaments move causing stretching at the end of the paired sections.

From these observations it can be expected that the detailed interactions of vortices become important for correct modelling of vortex stretching. It is noted here that the vorticity starts increasing rapidly at about $\underline{t} = 0.2$ when the filaments have rolled up so that some seprations are less than δ and the future evolution of the vorticity will depend on the form of the smoothing function.

We can study the spatial intermittency of the flow by studying the amount of vortex stretching that occurs and its distribution. Fig 6 shows histograms of enstrophy and volume against the stretching factor for the individual filament segments at the end of the integration. A very small fraction of the filaments have stretched by a factor of more than 10^5 whereas other parts have compressed slightly. The most highly stretched segments with high enstrophy, $L_2(\omega)$ occupy a very small fraction of the total volume, an indication of intermittency.

4.4 Effect of altering the smoothing function

A trial integration was run with the value of δ allowed to vary with the radius of the segments. Each segment used in the velocity calculations was assigned a value of δ equal to the radius determined from the amount of stretching it had undergone. At a given time

$$Rad_{ij} = (V_{ij}/\pi\lambda_{ij})^{1/2} \qquad (43)$$

where Rad_{ij} is the radius of the jth segment on the ith filament.

Initially the radius of all segments $Rad_{ij} = 0.05$. The rest of the parameters in Chorin's method were as in the standard integration. The results showed a far more rapid increase in vorticity after $t = 0.188$ than for the standard integration, see Fig 2 curve B. The integrations could not be followed for a long period of time because of the far higher induced velocities, the maximum reaching 347 ms^{-1} by $t = 0.224$ as opposed to a maximum of 5.2 ms^{-1} in the standard integration at $t = 0.333$. However the increase in velocity is not steady, nor that of $L_1(\omega)$ and $L_2(\omega)$. After $t = 0.191$ oscillations occurred in all three

values and continued for about 68 steps, the timestep being reduced at step 197, by this time the kinetic energy had increased so that the calculation was probably unreliable.

In order to increase the accuracy of the method another run was undertaken with a reduced value of $\underline{F} = 0.002$, thus providing better temporal resolution when the velocities increased. The maximum segment length $\lambda_{\underline{m}}$ was also made to vary with the segment radius so that $\lambda_{\underline{m}\underline{i}}{}^{\underline{j}} = \underline{\text{Rad}}_{\underline{i}}{}^{\underline{j}}$ thus providing better spatial resolution and allowing more accurate representation of small radii of curvature. This run showed an even more rapid increase in vorticity, see Fig. 2 curve c, and diverged from the $\underline{F} = 0.03$, constant $\lambda_{\underline{m}}$ solution at about $\underline{t} = 0.186$ when the vorticity increased sharply. The configuration was much smoother and the velocity, $\underline{L}_1(\omega)$ and $\underline{L}_2(\omega)$ increased without oscillations. The velocity reached a value of 188 ms^{-1} at $\underline{t} = 0.18874$. Over the next three steps the velocity increased to 1028 ms^{-1} indicating that by that stage even this solution had lost accuracy and obviously this test case is very unstable.

The evolution of the configuration of the filaments also differed from that for constant δ, see Fig. 7. The rapid stretching occurs at a different part of the filament but is again associated with dipole pairing between the filaments. The filaments being more tightly paired and folded than for equivalent values of $\underline{L}_1(\omega)$ at later times when δ is kept constant. Nearly all the extra vorticity above that in the standard integraiton can be accounted for in very small scale, highly stretched and dipole paired vorticity.

Now consider the comparison of the evolution of $\underline{L}_2(\omega)$ against $\underline{L}_1(\omega)$, see table IV. $\underline{L}_2(\omega)$ is higher for a given value of $\underline{L}_1(\omega)$ for variable δ at later times when the filaments have stretched. This implies that the stretching is less intermittent.

In this case, despite the smooth, apparently accurate solution and the tight dipole pairing seen in Fig. 7, the kinetic energy was not conserved. It increased from about 0.34 per unit value to 0.4 per unit volume by the end of the integration as calculated on an 80^3 grid.

A final test integration of Chorin's method used his form of the function $\underline{g}(\underline{a}/\delta)$ given by Eq. (8) corresponding to a vorticity distribution increasing from zero at δ to infinity on the line segments. Again in order to limit the number of image contributions to the velocity integral

$$\underline{g}(\underline{a}/\delta) = 0 \text{ when } |\vec{a}| > \underline{Rmax} \qquad (44)$$

The value of δ was kept constant as in the standard integration and δ = 0.05.

Again the evolution is similar to the standard integration until about $\underline{t}$ = 0.15 when $\underline{L}_1(\omega)$ and $\underline{L}_2(\omega)$ increase more rapidly, see Fig. 2. Vortex pairing is observed, although the configuration is different from the standard integration, compare Fig. 8 and Fig. 1. But this time the rapid stretching occurs in the same region as for the standard integration.

After $\underline{t}$ = 0.2 $\underline{L}_2(\omega)$ is lower for a given $\underline{L}_1(\omega)$ than in the standard integration indicating that the stretching is more intermittent, see table IV. The kinetic energy is again increasing slightly by the end of the integration so that the results may not be reliable after $\underline{t}$ = 0.3.

4.5 Investigation of the singularity of Euler's Equations

If the vorticity is to become singular in finite time the rate of increase of the $\underline{L}_1$ norms of vorticity must be greater than an exponential increase. Hence by considering

$$\underline{L}_1(\omega,\underline{t}) = \underline{L}_1(\omega,o)\ \exp\ (\underline{t}/\tau) \tag{45}$$

where τ is constant

$$\frac{d\underline{L}_1(\omega,\underline{t})}{d\underline{t}} = \frac{\underline{L}_1(\omega,\underline{t})}{\tau} \tag{46}$$

$$\underline{R}_{\underline{L}_1} = \frac{d\underline{L}_1(\omega,\underline{t})}{d\underline{t}} \Big/ \underline{L}_1(\omega,\underline{t}) = \frac{1}{\tau} = \text{constant} \tag{47}$$

If the ratio $\underline{R}_{\underline{L}_1}$ of the rate of change of the $\underline{L}_1$ norm to the $\underline{L}_1$ norm increases with time the vorticity is increasing at a rate faster than exponential. By considering table V it seems that for the standard integration of Chorin's method the ratio increases until about $\underline{t} = 0.26$, when it becomes roughly constant until approximately $\underline{t} = 0.36$. Then it begins increasing again. The results are confirmed when the full resolution of the 0.001 timestep is used.

A similar analysis of the $\underline{L}_2$ norms shows that

$$\underline{R}_{\underline{L}_2} = \frac{d\underline{L}_2(\omega,\underline{t})}{d\underline{t}} \Big/ \underline{L}_2(\omega,\underline{t}) \tag{48}$$

increases until $\underline{t} = 0.22$ and then begins decreasing.

Thus the rate of increase of the vorticity norms are greater than exponential until about $\underline{t} = 0.2$ and the solution is tending to a singularity. However after that the behaviour alters and the rates of increase decline.

The changes in rates of increase of $\underline{L}_1(\omega)$ and $\underline{L}_2(\omega)$ are confirmed by studying the convergence properties of the series of doubling incremental times.

Now consider the convergence properties of the series of time increments for equal intervals of $\underline{L}_1(\omega)$ or $\underline{L}_2(\omega)$ for the standard integration. The indications from the first two studies of a change in behaviour at times greater than $\underline{t} = 0.2$ suggests that we consider only the interval before $\underline{t} = 0.2$. Since $\underline{L}_1(\omega) = 3.2$ at $\underline{t} = 0.2$ we use $\Delta\underline{L}_1 = 0.1$ and the results are shown in table VI. These suggest that from $\underline{t} = 0.104$ up to $\underline{t} = 0.196$ the ratio of consecutive time increments could be considered constant, to within the accuracy of the method, at a value of 0.8. This indicates a converging series from the ratio test. After $\underline{t} = 0.196$ the ratio starts tending towards 1 which indicates a diverging series. However, by this time the time resolution is insufficient to provide reasonably accurate values of the ratios. Also, since the solutions in section 4.4 diverged after about $\underline{t} = 0.18$ when different forms of smoothing function were used the results after this time are unreliable. In particular the effect of using a constant width smoothing function reduced the amount and rate of stretching by limiting the magnitudes of strain in the flow.

If we assume that the series of time increments for constant $\Delta\underline{L}_1$ can be continued with a constant ratio of 0.8 beyond $\underline{t} = 0.18$ we obtain a geometric series with a finite limit $\underline{t}^*$ as the time of the singularity

$$\underline{t}^* = \underline{t}_o + \underline{t}_1 \sum_{\underline{n}=0}^{\infty} \underline{q}^{\underline{n}} \qquad (49)$$

with $\underline{t}_o = 0.104$, $\underline{t}_1 = 0.024$, $\underline{q} = 0.8$

$$\underline{t}^* = \underline{t}_o + \frac{\underline{t}_1}{1-\underline{q}} = 0.224 \qquad (50)$$

This receives support in the results of the variable δ calculation where the $\underline{L}_1$ norm increases very rapidly in a short period before this time.

Further insight can be obtained by using Eq (49)

$$\text{where the increments } \underline{t}_1\underline{q}^{\underline{n}} = \int_{\underline{L}_o + \underline{n}\Delta\underline{L}}^{\underline{L}_o + (\underline{n}+1)\,\Delta\underline{L}} \underline{f}(\underline{L})\,d\underline{L} \qquad (51)$$

with $\underline{L}_o = \underline{L}_1(\omega)$ at time $\underline{t}_o$

$\Delta\underline{L} = \Delta\underline{L}_1$

$\underline{L} = \underline{L}_1(\omega)$ at time $\underline{t}$

$$\text{we find that } \underline{f}(\underline{L}) = \left(\frac{\underline{t}_1 \log(\underline{q})}{\Delta\underline{L}(\underline{q}-1)}\right) \cdot \underline{q}^{\eta(\underline{L})} \qquad (52)$$

where $\eta(\underline{L}) = (\underline{L}-\underline{L}_o)/\Delta\underline{L}$

$$\text{so that } \underline{t} = \underline{t}_o + \frac{\underline{t}_1 \log(\underline{q})}{\Delta\underline{L}(\underline{q}-1)} \int_{\underline{L}_o}^{\underline{L}'} \underline{q}^{\eta(\underline{L})}\, d\underline{L} \qquad (53)$$

$$\text{giving } \underline{t} = \underline{t}_o + \frac{\underline{t}_1}{1-\underline{q}} + \left(\frac{\Delta\underline{L}}{\log(\underline{q})}\right)\frac{d\underline{t}}{d\underline{L}} \qquad (54)$$

Hence a geometric series for the time increments implies an inverse linear relationship between time and $d\underline{L}_1(\omega)/d\underline{t}$ with $\underline{t}^*$ being defined as the point where $d\underline{t}/d\underline{L}_1(\omega) = 0$. Fig. 9 shows $\underline{t}$ against $\Delta\underline{t}/\Delta\underline{L}_1, \Delta\underline{t}/\Delta\underline{L}_2$ for δ = const and $\Delta\underline{t}/\Delta\underline{L}_2$ for variable $\delta, \lambda_{\underline{m}}$ and $\underline{F} = 0.002$. We find that for all three curves the gradient increases until $\underline{t} = 0.08$. Consider the curves for δ = const after $\underline{t} = 0.08$, the relationship becomes nearly linear although the gradient decreases slightly between $\underline{t} = 0.13$ and $\underline{t} = 0.15$ before becoming constant again. After $\underline{t} = 0.18$ the gradient

increases rapidly. Straight lines drawn through the data for $\underline{t}$ = 0.08 to 0.18 give $\underline{t}^*$ = 0.19 and 0.2 respectively for the $\underline{L}_1(\omega)$ and $\underline{L}_2(\omega)$ curves.

In the case of variable δ the gradient decreases after $\underline{t}$ = 0.1 until $\underline{t}$ = 0.18, when it begins to increase rapidly. An asymoptic continuation of the decreasing gradient would give $\underline{t}^*$ = 0.183.

These results again indicate a change in the nature of the solution after $\underline{t}$ = 0.18.

5. DISCUSSION

5.1 Dependence of the solution on the smoothing function

The results of the integrations using Chorin's method show that the evolution of the flow is dependent on the form of the function $\underline{g}(\underline{a}/\delta)$. The solutions diverge markedly after about $\underline{t}$ = 0.18 by which time the separation of some non-consecutive segments has become less than δ and the details of the interactions between the vortices have become important. The forms of these motions are very dependent on the smoothing function used in the velocity integral and, in reality, on the core structure of the filaments.

Chorin [4] using $\underline{g}(\underline{a}/\delta) = \underline{a}^2/\delta^2$ states that when δ was allowed to vary, as in section 4.4 the $\underline{L}_1(\omega)$, $\underline{L}_2(\omega)$ relationship was unaltered. The results reported here do not confirm Chorin's result. The non conservation of kinetic energy in the variable δ solution is a puzzling feature as the solution appears accurate and the dipole pairs are very close. It is possible that the use of a cutoff δ varying with local segment stretching is not consistent with the conservation of energy in single filament calculations. The changes in core shape and vorticity distribution, that cannot be represented, may be important in

determining the exact amount of stretching consistent with energy conservation. Obviously the calculation of energy on a grid may not be accurate enough to cope with the fine scale structure and localized high velocities of the variable δ solution. But the energies calculated on both a 20^3 and 80^3 grid show the increase in energy. It is also possible that a varying but uniform value of δ should be used for the whole filament if internal waves smooth out variations along the length [18] and this may improve the conservation of energy.

The results of the integrations of Beale and Majda's method described in section 4.2 imply that for single filament calculations the solution is solely determined by the circulation of the filaments and the width of the smoothing function. The effective cross-section resolution only seems to determine the accuracy of the solution. This, plus the results of sections 4.1 and 4.4 support the conclusions of Greengard [14] that we are studying the convergence of solutions to the E_δ equations. This is backed by further comparison integrations to $\underline{t}$ = 0.2 using differing $\underline{g}(\underline{a}/\delta)$ in both Chorin's and Beale and Majda's methods. It was found that the evolution was very dependent on δ and to a smaller extent on the form of the function $\underline{g}(\underline{a}/\delta)$. Also large values of δ, much greater than $\underline{h}$ or $\lambda_{\underline{m}}$, produced smoother solutions, perhaps inhibiting the production of short wavelength features along the length of the filaments. Small values of δ, less than $\underline{h}$ or $\lambda_{\underline{m}}$ gave instabilities. Thus we conclude that for single filament calculations the solutions converge to those of the E_δ equations as resolution is improved, the form of the solution depending on the form of the smoothing function $\underline{g}(\underline{a}/\delta)$ and the value of δ. Trials were run with a vortex ring configuration, with non periodic boundaries and using

different values of δ and $\underline{g}(\underline{a}/\delta) = \tanh(\underline{a}^3/\delta^3)$. The results indicate that if the resolution is sufficiently high, the resultant velocities of translation of the ring approximate those of a ring with uniform vorticity distribution in a cross-section of radius δ. We conclude that for all single filament calculations the function $\underline{g}(\underline{a}/\delta)$ should be considered as representing the internal structure of a vortex tube, with δ related to the cross-section of the core, so that the initial data is well defined. Single filament calculations should not be considered as the low resolution limit of filament bundle or discrete vortex methods but as very different methods.

From the results of the variable δ calculation we conclude that the use of a constant width smoothing function results in smoothing of interactions so that small scale structure is removed and hence the rates of increase of $\underline{L}_1(\omega)$ and $\underline{L}_2(\omega)$ are reduced. Thus the amount of vortex stretching can be underestimated and the properties of the flow such as intermittency misrepresented. Thus the solution of the E_δ equations for single filaments may be smoothed forms of the Euler equations as the second order effects of compression and stretching along the lengths of filaments are mistreated. The solutions are probably only accurate whilst the separations of filaments and their radii of curvature are greater than δ.

Obviously the accuracy of the variable δ calculations as solutions of the Euler equations has not been proved and multiple filament calculations are probably required to study the effects of the deatils of the core dynamics on the vortex interations.

Once the structure of the core can be resolved by bundles of filaments or arrays of discrete vortices, the individual elements can represent velocity gradients and structures below the resolution of the cutoff length δ. δ can then remain constant and purely provide stability.

Initial trials with a bundle of five or seven filaments per vortex produced extra vorticity, due to twisting of the outer filaments around one on the axis of the vortex, when δ was about 1.5 times the spacing of the filaments. When δ was four times the spacing the twisting was suppressed. Solutions were very sensitive to the spacing of the filaments and the relationship between that and the value of δ.

5.2 Vortex Dipole Pairing

Despite the variations in the solutions obtained for the evolution of this vortex lattice they all showed that vortex dipole pairing occurred in the region of the cross over of two filaments. Two different situations here have produced dipole pairing and rapid vortex stretching. In the case of variable δ it is simply a mutual interaction between the two filaments. In the case of constant δ it is a self interaction on each of the filaments as a result of folding of one filament as it twists around the other. The dipole pairing can be considered to be a necessary feature of the flow if vorticity is to increase whilst conserving energy.

This feature suggests a plausible method of parametrizing the effects of viscosity in vortex filament calculations by removing any dipole paired sections of filaments and relinking the remainder. This can be justified because in these regions the diffusive effects of viscosity will be most effective since the vorticity density and hence

velocity gradients are very high. The two cores of opposite signed vorticity can be expected to diffuse into each other and result in zero net vorticity. They are also associated with highly stretched vorticity and hence the smallest scales of motion. The cancellation of velocity fields means that the large scale flow and evolution of unpaired vorticity should be largely unaffected by the details of the evolution of the highly stretched, tangled or dipole paired vorticity.

This mechanism is consistent with the observations of the interactions of trailing vortices and vortex rings [21, 22]. These suggest that vorticity can merge and relink. The need to change the topology of interacting vortex filaments has been widely recognised and Leonard [2, 3] implemented a reconnection method as did Schwarz [24] in the collisions of vortex filaments is superfluid helium.

Feynman [25] suggested that annihilation of lengths of filaments and relinking should occur if situations equivalent to dipole pairing arise in the fluid. Schwarz [24] implements a scheme for relinking filaments if vortex lines cut across each other in his use of the local induction approximation [26]. This method does not allow for interactions between filaments and so cannot produce the interactions seen in the solutions here. The results reported here for variable δ reconcile the two different schemes of Feynman and Schwarz since the vortex lattice starts as vortex lines crossing and the mutual interactions result in dipole pairing of vorticity.

Obviously further numerical, theoretical or analytical calculations are required to produce a vigorous verification of dipole pairing and its importance in the process of rapid stretching of vorticity whilst conserving energy. This work was completed before the paper by Siggia

(27) was brought to our attention. His integrations provide additional, independent evidence for the collapse of vortex filaments to a singularity as a result of vortex dipole pairing.

5.3 Singularity of the Euler Equations

Unfortunately the investigations reported in section 4.5 could not provide a conclusive result. The findings indicate a change in the nature of the solutions after $\underline{t} = 0.18$ when the separations of non-consecutive segments become less than the cutoff parameter $\delta = 0.05$.

We can suggest two possible explanations. One is that the true solution of the Euler equatons does become singular in finite time at about $\underline{t}^* = 0.2$ The numerical solutions losing accuracy and not able to reproduce the rapid rate of stretching after about $\underline{t} = 0.18$.

A second suggestion is that we are seeing intermittency in the flow and the singularity does not occur. There is no reason why we should expect the flow to follow a smooth easily defined solution.

We feel that, since the character of the solution changes once the approximations and smoothing become important, the results are consistent with the presence of a singularity.

Chorin [3] used rescaling in order to investigate the properties of the flow resulting from intersecting vortex loops. Thus although a constant value of δ was used in each rescaled flow the value was effectively reduced by each rescaling. Hence he was concentrating on ever decreasing scales of motion and probably provided a solution intermediate between a constant and variable δ solution.

6. CONCLUSION

The results from the integrations using Chorin's three dimensional vortex method produce a solution that is only weakly dependent on the time integration scheme, time step, resolution of the initial data, maximum segment length and distant contributions to the velocity integral. The comparison with the solutions obtained using Beale and Majdas method illustrate the similarity of the two schemes.

The solutions were found to be very dependent on the form and width, δ, of the smoothing function used in the velocity integral. In particular solutions diverged once the separations of different sections of the filaments becomes less than the cutoff width δ, illustrating the fact that the detailed interactions become important for the correct modelling of vortex stretching. Thus any deduced properties of turbulent flow are likely to be dependent on the form of the smoothing function used. In particular use of constant cutoff width underestimated the rate of increase of vorticity assuming that the solution for variable δ is closer to the true solution. Short wavelength features and second order effects due to changes in the cross-section radius of a real vortex are smoothed out. This may not be the same as the effects of viscosity in that it is not dispersive but it certainly removes small scale structure. The calculations need to be extended to increase resolution in the cross-section of the vortices so that a single vortex is represented by a bundle of filaments or array of vortex elements. This will aid understanding of the situation being modelled by a single filament with a given smoothing function and width.

It is then important to ensure that a bundle does not act as separate vortices and great care is required in the choice of the smoothing function and its width to ensure stability and convergence.

The evolution of the periodic lattice of vortex filaments shows a rapid increase with time of the $\underline{L}_1$ and $\underline{L}_2$ norms of vorticity. This indicates the presence of a singularity in finite time but the results are not conclusive as discussed in section 5.3.

Possibly the most important product of this study is that the mechanism of a vortex dipole pairing, identified by Chorin [4] as being necessary in order to conserve energy, may in fact be responsible for the rapid increase in vorticity. This also suggests a method for the parametrization of the effects of viscosity by removing the cancelling sections and relinking the remainder.

ACKNOWLEDGEMENTS

I wish to thank Mr M Holt who produced the computer code for the implementation of Beale and Majda's method and Professor Chorin for the use of his method and many helpful comments on this work. I also with to thank Professors A. Majda, A. Leonard and D. W. Moore and Dr Greengard for their comments on my work and Dr M Cullen for suggesting this study and for his help and encouragement.

REFERENCES

1. A LEONARD J. Comput. Phys. 37 (1980), 289-335.

2. A LEONARD Ann. Rev. Fluid Mech. 17 (1985), 523-559.

3. A J CHORIN Commun. Pure Appl. Math. 34 (1981), 853-866.

4. A J CHORIN Commun. Math. Phys. 83 (1982), 517-535.

5. J T BEALE and A MAJDA Math. Comput. 39 (1982), 1-27.

6. C ANDERSON and C A GREENGARD SIAM J. Numer. Anal 22 (1985), 413-440.

7. R F MORF, S A ORSZAG and U FRISCH Phys. Rev. Lett 44 (1980) 572-575.

8. M E BRACHET, D I MEIRON, S A ORSZAG, B G NICKEL, R H MORF and U. FRISCH J. Fluid Mech. 130 (1983), 411-452.

9. D W MOORE Aeronaut. Q. 23 (1972), 307-314.

10. S E WIDNALL, D BLISS and A ZALAY in "Aircraft Wake Turbulence and its Detection" p 305-338, Plenum, New York, 1971.

11. A LEONARD in "Turbulent Shear Flows 2" p 66-77, Springer-Verlag, Berlin/Heidelberg, 1980.

12. A J CHORIN SIAM J Sci. Stat. Comput. 1 (1980), 1-21.

13. S SHIRAYAMA and K KUWAHARA in "Proc. Int. Conf. Numer. Meth. Fluid Dyn., 9th, June 1984, Suclay, France" to be published by Springer-Verlag in Lecture Notes in Physics.

14. C A GREENGARD, Ph. D. Thesis, University of California at Berkeley (1984).

15. J T BEALE and A MAJDA Math. Comput. 39 (1982), 29-52.

16. A J CHORIN and J MARSDEN "A Mathematical Introduction to Fluid Mechanics" Springer-Verlag, New York, 1979.

17. S C CROW AIAA J. 8 (1970), 2172-2179.

18. D W MOORE and P G SAFFMAN Phil. Trans. R. Soc. London Ser. A 272 (1972), 403-429.

19. O H HALD SIAM J. Numer. Anal 16 (1979), 1726-1755.

20. J T BEALE and A MAJDA "Explicit Smooth Velocity Kernels for Vortex Methods" MRC Technical Summary Report No. 2480, University of Wisconsin-Madison.

21. T FOHL and J S TURNER Phys. Fluids 18 (1975), 433-436.

22. T SARPKAYA J. Fluid Mech 136 (1983), 85-109.

23. A LEONARD in "Proc Int. Conf. Numer. Meth. Fluid Dyn., 4th, Colo.", pp 245-250, Springer-Verlag, Heidelberg, 1975.

24. K W SCHWARZ Phys. Rev. Lett. 49 (1982), 283-285.

25. R P FEYNMAN Prog. Low Temp. Phys. 1 (1957), 17-53.

26. F R HAMA Phys. Fluids 5 (1962), 1156-1162.

27. E D SIGGIA Phys. Fluids 28 (1985) 794-805.

Figure Legends

FIG. 1. Evolution of the configuration of the vortex filaments from the standard integration of Chorin's method. a) $\underline{t} = 0.0$, b) $\underline{t} = 0.2$, c) $\underline{t} = 0.25$, d) $\underline{t} = 0.3$

o initial nodes on filament A.

Δ initial nodes on filament B.

FIG. 2. Evolution of the $\underline{L}_1$ norm of vorticity. Curves A to D are Chorin's method. Curve A is the standard integration, Curve B has $\delta = \underline{Rad}_i\underline{j}$, Curve C has $\lambda_{\underline{m}} = \delta = \underline{Rad}_i\underline{j}$ and $\underline{F} = 0.002$ and Curve D uses $\underline{g}(\underline{a}/\delta) = \underline{a}^2/\delta^2$. Curves E to H are Beale and Majda's method with $\underline{h} = 0.003125$, 0.0125, 0.025 and 0.05 respectively.

FIG. 3. Comparison of the plan views of the configuration of the filaments at $\underline{t} = 0.2$ from integrations of Beale and Majda's method with different resolutions. → Magnitude and direction of vorticity vector in X-Y plane scaled so that the initial magnitude = $\underline{h}$.

For $\underline{h} = 0.05$ to 0.0125 o vorticity component into paper

\+ vorticity component out of paper.

FIG. 4. Plan views of the configuration of the filaments at $\underline{t} = 0.25$ and $\underline{t} = 0.3$ from the integration of Beale and Madja's method with $\underline{h} = 0.003125$. → Magnitude and direction of vorticity vector in X-Y plane.

FIG. 5. 3-D representation of the configuration of the vortex filaments at $\underline{t}$ = 0.3 for standard integration using Chorin's method showing vortex dipole pairing.

——— Filament A - - - Filament B

→ direction of vorticity vector.

FIG. 6. Histograms of enstrophy and volume per 0.2 interval of $\log_{10}(\underline{S})$ at $\underline{t}$ = 0.398 for the standard integration of Chorin's method.

$\underline{S}$ = stretching factor = $\lambda_{\underline{i}}\underline{j}\pi\underline{r}_o^2/\underline{V}_{o\underline{i}}\underline{j}$ and enstrophy = $\underline{L}_2(\omega)$

- - - - volume

——— enstrophy.

FIG. 7. Plan and side views and 3-D representation of the configuration of the vortex filaments at $\underline{t}$ = 0.18871 after 200 steps from the integration using Chorin's method with variable $\delta = \lambda_{\underline{m}} = \underline{Rad}_{\underline{i}}\underline{j}$ and $\underline{F}$ = 0.002.

o initial nodes on filament A

Δ initial nodes on filament B

——— Filament A - - - - Filament B

→ direction of vorticity vector.

FIG. 8. Evolution of the configuration of the vortex filaments from the integration using Chorin's method with $\underline{g}(\underline{a}/\delta) = \underline{a}^2/\delta^2$.

a) $\underline{t}$ = 0.2, b) $\underline{t}$ = 0.25, c) $\underline{t}$ = 0.3

x initial nodes on filament A

o initial nodes on filament B

——— Filament A - - - - - Filament B

FIG. 9. Relationship between time and $\Delta t/\Delta L_1(\omega)$ and $\Delta t/\Delta L_1(\omega)$. Curve A is $\Delta t/\Delta L_1(\omega)$ for the standard integration, Curve B is $\Delta t/\Delta L_2(\omega)$ for the standard integration and Curve C is $\Delta t/\Delta L_2(\omega)$ for the integration using variable $\delta = \lambda_m = \text{Rad}_i^j$.

TABLE I

Evolution of $L_1(\omega)$ and $L_2(\omega)$ from Chorin's method for different values of the adjustable parameters [a]

	Standard integration		$\lambda_{oi}{}^j = 0.05$		$\lambda_m = 0.0125$		$F = 0.002$		Rmax = 0.995		$\lambda_{oi}{}^j = 0.05$ Rmax = 999.0 27 nearest images	
Time, t	$L_1(\omega)$	$L_2(\omega)$[b]	$L_1(\omega)$	$L_2(\omega)$[b]	$L_1(\omega)$	$L_2(\omega)$[b]	$L_1(\omega)$	$L_2(\omega)$[b]	$L_1(\omega)$	$L_2(\omega)$[b]	$L_1(\omega)$	$L_2(\omega)$[b]
0.0	2.0	2.6×10^2	2.0	2.6×10^2	2.0	2.6×10^2	2.0	2.6×10^2	2.0	2.6×10^2	2.0	2.6×10^2
0.05	2.1	2.8×10^2	2.1	2.8×10^2	2.1	2.8×10^2	2.1	2.8×10^2	2.1	2.8×10^2	2.1	2.8×10^2
0.10	2.2	3.5×10^2	2.2	3.5×10^2	2.2	3.5×10^2	2.2	3.5×10^2	2.2	3.4×10^2	2.2	3.5×10^2
0.15	2.4	4.9×10^2	2.5	5.0×10^2	2.4	4.8×10^2	2.4	4.9×10^2	2.4	4.7×10^2	2.5	5.0×10^2
0.20	3.2	1.3×10^3	3.3	1.3×10^3	3.1	1.2×10^3	3.2	1.3×10^3	3.1	1.1×10^3	3.3	1.2×10^3
0.25	6.1	1.5×10^4	6.1	1.2×10^4	6.0	1.3×10^4	6.1	1.5×10^4	5.9	1.2×10^4		
0.30	13.2	1.1×10^5	13.3	1.2×10^5	12.6	8.9×10^4	13.2	1.1×10^5	12.4	9.2×10^4		
0.35	28.4	9.3×10^5	31.8	9.2×10^5					26.6	8.1×10^5		
0.39	55.8	7.3×10^6	64.3	6.3×10^6					51.4	5.3×10^6		

[a] All integrations used a 4th order Runge-Kutta time integration scheme and $g(a/\delta) = a^3/\delta^3$ with $\delta = 0.05$. The standard integration had unequal $\lambda_{oi}{}^j$, $\lambda_m = 0.05$, $F = 0.03$, Rmax = 0.495 and $dt = 0.001$. The other integrations used the standard values apart from those shown in the column headings. Not all integrations were run to $t = 0.39$.

[b] Using $r_o = 0.05$.

TABLE II

Evolution of $L_1(\omega)$ and energy from

Chorin's method using different time integration schemes[a]

	4th order Runge-Kutta		Centred Difference		Centred Difference with filtering[b]		Euler forward Difference	
Time,t	$L_1(\omega)$	Energy[c]	$L_1(\omega)$	Energy[c]	$L_1(\omega)$	Energy[c]	$L_1(\omega)$	Energy[c]
0.0	2.0	0.35	2.0	0.35	2.0	0.35	2.0	0.35
0.1	2.2	0.34	2.2	0.34	2.2	0.34	2.2	0.34
0.2	3.2	0.33	3.2	0.33	3.2	0.33	3.2	0.33
0.3	13.2	0.34	13.3	0.34	12.9	0.33	12.5	0.34
0.35	28.4	0.33	36.4	0.55	28.5	0.34	29.9	0.35
0.36	33.2	0.33	51.0	0.82	38.2	-	36.3	-
0.39	55.8	0.34			56.1	0.35	65.4	0.38
0.398	64.8	0.34			64.7			

[a] All integrations used $g(a/\delta) = a^3/\delta^3$, $\delta = 0.05$, unequal $\lambda_{oi}{}^j$, $\lambda_m = 0.05$, $F = 0.03$, Rmax = 0.495 and dt = 0.001. Not all integrations were run to $t = 0.398$.

[b] weighting factor $\zeta = 0.1$

[c] calculated on a 20^3 grid at selected times.

TABLE III

Evolution of $L_1(\omega)$ and $L_2(\omega)$ from Chorin's method and Beale and Majda's method at different resolutions.[a]

	Chorin's Method [b]		Beale and Majda's method							
			h = 0.003125		h = 0.0125		h = 0.025		h = 0.05	
Time,t	$L_1(\omega)$	$L_2(\omega)$[c]	$L_1(\omega)$	$L_2(\omega)$[d]	$L_1(\omega)$	$L_2(\omega)$[d]	$L_1(\omega)$	$L_2(\omega)$[d]	$L_1(\omega)$	$L_2(\omega)$[d]
0.00	2.0	2.6×10^2	2.0	2.0×10^5	2.0	1.3×10^4	2.0	3.2×10^3	2.0	8.0×10^2
0.05	2.1	2.8×10^2	2.1	2.3×10^5	2.1	1.4×10^4	2.0	3.5×10^3	2.0	8.6×10^2
0.10	2.2	3.5×10^2	2.2	2.8×10^5	2.2	1.7×10^4	2.2	4.3×10^3	2.2	1.0×10^3
0.15	2.4	4.9×10^2	2.4	3.8×10^5	2.4	2.3×10^4	2.4	5.4×10^3	2.3	1.2×10^3
0.20	3.2	1.3×10^3	3.1	8.7×10^5	2.9	3.8×10^4	2.7	7.3×10^3	2.5	1.5×10^3
0.25	6.1	1.5×10^4	5.6	5.5×10^6	4.2	1.1×10^5	3.3	1.1×10^4	2.8	1.8×10^3
0.30	13.2	1.1×10^5	9.1	1.7×10^7	6.0	2.6×10^5	4.1	1.7×10^4	3.1	2.1×10^3
0.35	28.4	9.3×10^5	16.3	4.9×10^7	7.9	4.5×10^5	4.6	2.2×10^4	3.6	2.9×10^3
0.398	64.8	1.2×10^7	27.9	1.1×10^8	9.1	5.2×10^5	5.2	3.0×10^4	4.0	3.7×10^3
0.40	-	-	28.4	1.1×10^8	9.2	5.3×10^5	5.2	3.0×10^4	4.1	3.8×10^3

[a] All integrations used a 4th order Runge-Kutta time integration scheme and $g(a/\delta) = a^3/\delta^3$ with $\delta = 0.05$.

[b] Results shown are from the standard integration.

[c] Using $r_o = 0.05$.

[d] Values given should be multiplied by $127 \times h^2$ for direct comparison with Chorin's method.

TABLE IV

Variation of $L_2(\omega)$ with $L_1(\omega)$ from Chorin's method with different smoothing functions [a]

$g(a/\delta) = a^3/\delta^3$ δ = constant = 0.05[b]			$g(a/\delta) = a^3/\delta^3$ $\lambda_m = \delta$ = variable = Rad_i[j] F = 0.002			$g(a/\delta) = a^2/\delta^2$ δ = constant = 0.05		
$L_1(\omega)$	$L_2(\omega)$	time	$L_1(\omega)$	$L_2(\omega)$	time	$L_1(\omega)$	$L_2(\omega)$	Time
2.0	2.55×10^2	0.0	2.0	2.55×10^2	0.0	2.0	2.55×10^2	0.0
2.09	3.01×10^2	0.068	2.09	3.02×10^2	0.070	2.09	3.00×10^2	0.068
2.42	4.87×10^2	0.150	2.41	4.96×10^2	0.160	2.41	5.01×10^2	0.150
2.60	5.99×10^2	0.170	2.60	6.57×10^2	0.180	2.60	6.41×10^2	0.169
2.96	9.13×10^2	0.191	2.94	1.51×10^3	0.187	2.94	9.37×10^2	0.184
3.16	1.18×10^3	0.198	3.14	3.67×10^3	0.188	3.17	1.19×10^3	0.190
5.05	7.94×10^3	0.235	4.7	6.61×10^5	0.1887	5.12	5.86×10^3	0.219
12.01	8.92×10^4	0.294				12.02	6.81×10^4	0.269
66.0	1.33×10^7	0.399				67.2	4.69×10^6	0.341

[a] All integrations were based on the standard integration [b] with the differences shown in the column headings.

TABLE V

Evolution of $\frac{dL_1(\omega)}{dt} / L_1(\omega)$ [a]

Time, t	$L_1(\omega)$	$\Delta L_1(\omega)$[b]	$\frac{\Delta L_1(\omega)}{\Delta t} / L_1(\omega)$[c]
0.02	2.008	0.032	0.398
0.04	2.032	0.064	0.787
0.06	2.072	0.088	1.06
0.08	2.12	0.118	1.39
0.1	2.19	0.14	1.60
0.12	2.26	0.17	1.88
0.14	2.36	0.24	2.54
0.16	2.5	0.38	3.8
0.18	2.74	0.72	6.57
0.2	3.22	1.4	10.8
0.22	4.14	2.16	13.0
0.24	5.38	2.92	13.6
0.26	7.06	4.32	15.3
0.28	9.7	6.14	15.8
0.3	13.2	8.2	15.5
0.32	17.9	11.0	15.4
0.34	24.2	15.3	15.8
0.36	33.2	22.3	16.8
0.38	46.5	32.8[d]	18.1[e]

a $\frac{dL_1(\omega)}{dt} / L_1(\omega)$ is approximated by $\frac{\Delta L_1(\omega)}{\Delta t} / L_1(\omega)$

values of $L_1(\omega)$ are from the standard integration of Chorin's method.

b $\Delta L_1(\omega) = L_1(\omega, t+0.02) - L_1(\omega, t-0.02)$

c $\Delta t = 0.04$

d $\Delta L_1(\omega) = L_1(\omega, 0.399) - L_1(\omega, 0.36)$

e $\Delta t = 0.039$.

TABLE VI

Convergence test for series Δt_n [a]

$L_1(\omega)_n$	Time, t [b]	Δt_n	ratio = $\frac{\Delta tn+1}{\Delta tn}$	Error in $L_1(\omega)$ [a]
2.0	0.0			0.0
		0.071		
2.1	0.071		0.46	-5.6×10^{-4}
		0.033		
2.2	0.104		0.73	1.4×10^{-3}
		0.024		
2.3	0.128		0.79	-1.1×10^{-3}
		0.019		
2.4	0.147		0.68	2.1×10^{-3}
		0.013		
2.5	0.160		0.77	-1.7×10^{-3}
		0.010		
2.6	0.170		0.80	-3.4×10^{-3}
		0.008		
2.7	0.178		0.75	1.4×10^{-3}
		0.006		
2.8	0.184		0.83	3.3×10^{-3}
		0.005		
2.9	0.189		0.80	9.1×10^{-3}
		0.004		
3.0	0.193		0.75	1.0×10^{-2}
		0.003		
3.1	0.196		1.0	-4.6×10^{-3}
		0.003		
3.2	0.199			-1.0×10^{-2}

a Results from the standard integration of Chorin's method with time resolution dt = 0.001.

b Times, t, are those that had $L_1(\omega,t)$ closest to the stated value $L_1(\omega)_n$

c Error = $L_1(\omega,t) - L_1(\omega)_n$

List of Symbols

In text vectors are shown using arrow notation but should be replaced by bold characters and characters that should be italic are underlined.

Symbol as shown in paper:	Phonetic description for appearance in journal
$\underline{L_1}$ or $\underline{L_1}(\omega)$	: Italic capital L, subscript figure one, small omega in parentheses.
$\underline{L_2}$ or $\underline{L_2}(\omega)$	: As above but subscript figure two.
$\frac{\underline{d}}{\underline{dt}}$	: Italic small d above time, Italic small d, small italic t below line.
$\frac{\underline{\partial}}{\underline{\partial t}}$	: Small delta above line, small delta, small italic t below line.
$\vec{\omega}$	: bold small omega
$\vec{u}$	: bold small u
∇	: del
0	: figure zero
∇^2	: del, superscript figure two.
π	: small pi
$\vec{x}$	: bold small x
$\vec{x}'$	: bold small x, superscript dash.
$\int \underline{d}\vec{x}'$	: Integral sign, small italic d, bold small x, superscript dash.
$\underline{t}$	: small italic t.
Γ	: Capital gamma
σ	: small sigma
$\underline{A}$	: Capital italic A
$\int_{\underline{A}} . d\vec{A}$	: Integral sign, subscript capital italic A, dot, small italic d, bold capital A.
$\underline{M}$	: Capital italic M
$\underline{\Gamma_i}$	: Capital gamma, subscript small italic i.
$\underline{g}(\underline{a}/\delta)$	: Small italic g, small italic a, slash, small italic delta in parenthesis.

$\underline{a}$: small italic a

δ : small delta

$\vec{a}$: small bold a.

$\underline{s}$: small italic s

$\underline{ds}$: small italic d, small italic s

$\vec{r}_{\underline{i}}(\underline{s})$: bold small r, subscript small italic i, small italic s in parentheses.

$\lambda_{\underline{m}}$: small lamda, subscript small italic m.

$\vec{x}_{\underline{m}}^{\underline{n}}$: bold small x, subscript small italic m, superscript small italic n.

$\vec{a}_{\underline{i}\underline{j}_{\underline{m}}}^{\underline{n}}$: small bold a, subcript small italic i, superscript small italic j, subcript small italic m, superscript n.

$\underline{N}_{\underline{i}}, \underline{N}_{\underline{m}}$: Capital italic N, subcript small italic i or m.

$\Delta\vec{s}_{\underline{i}}^{\underline{j}}$: Capital delta, small bold s, subscript small italic i, superscript small italic j

$\underline{j}'$: small italic j, superscript dash

$\vec{\alpha}$: bold small alpha

$\vec{x}_{\alpha}$: bold small x, subscript small alpha.

$\alpha_1, \alpha_2, \alpha_3$: small alpha, subscript figure one, two or three.

∇_{α} : Capital del, subscript small alpha

$\underline{h}$: Small italic h

$(\underline{lh}, \underline{mh}, \underline{nh})$: all small italic letters

$\vec{x}_{\underline{i}}, \vec{\alpha}_{\underline{i}}, \vec{\omega}_{\underline{i}}$: all bold small letters, subscript small italic i or j.

$\vec{u}_{\underline{i}}^{\underline{h}}(\underline{t})$: small bold u, subscript small italic i, superscript small italic h, small italic t in parentheses.

$\nabla_{\alpha}^{\underline{h}}$: del, subscript small alpha, superscript small italic h

$\underline{T}$: Capital italic T

$\vec{K}$: Bold capital K

ψ_{δ} : small psi, subscript small delta

$\vec{u}_{\delta}, \vec{K}_{\delta}, \vec{\omega}_{\delta}$: all bold letters with subscript small delta.

$\vec{dx}$: small italic d, bold small x.

x : small italic x

$*$: star

R : Capital italic R

q : small italic q

E_δ : Capital E, subscript small delta

z : small italic z

x_1, x_2, x_3 : small italic x, subscript figure one, two or three.

x : small italic x

y : small italic y

r_o : small italic r, subscript figure zero

$\vec{X}_A$: bold capital X, subscript capital A.

$\vec{X}_B$: bold capital X, subscript capital B.

u_1, u_2, u_3 : small italic u, subscript figure one, two or three

$Rmax$: Capital italic R, small italic max.

dt : small italic d, small italic t

P : Capital italic P

$umax$: small italic umax

F : Capital italic F

$\lambda_{oi}{}^{j}$: Small lamda, subscript figure zero, subcript small italic i, superscript small italic j.

$\vec{\omega}_A$, $\vec{\omega}_B$: Bold small omega, subscript capital A or B.

ω_o : small omega, subscript figure zero.

N : Capital italic N

m,n : small italic letters

dV : small italic d, Capital italic V

$L_1{}^{h}$, $L_2{}^{h}$: Capital italic L, subscript figure one or two, superscript small italic h.

L_1^c, L_2^c : Capital italic L, subscript figure one or two, superscript small c.

λ_i^j : small lamda, subscript small italic i, superscript small italic j.

V_i^j : Capital italic V, subscript small italic i, superscript small italic j

S_i^j : Capital italic S, subscript small italic i, superscript small italic j.

Δt : Capital delta, small italic t.

Rad_i^j : Capital italic R, small italic 'ad', subcript i, superscript j.

$L_1(\omega,t)$, $L_1(\omega,o)$: Capital italic L, subscript figure one or two, small omega and small italic t or figure zero in parentheses.

τ : small tau

R_{L_1}, R_{L_2} : Capital italic R, subscript capital italic L with subscript figure one or two.

ΔL_1 : Capital delta, capital italic L subscript figure one.

t^* : small italic t, superscript star.

t_o, t_1 : small italic t, subcript figures zero or one.

L_o : Capital italic L subscript figure zero.

ΔL : Capital delta, capital italic L.

$f(L)$: Small italic f, capital italic L in parentheses.

dL : small italic d, capital italic L

L' : Capital italic L, superscript dash.

q^n : small italic q, superscript small italic n

$\log(q)$: small letters log, small italic q in parentheses.

$\eta(L)$: small eta, capital italic L in parentheses.

$q^{\eta(L)}$: small italic q, superscript $\eta(L)$.

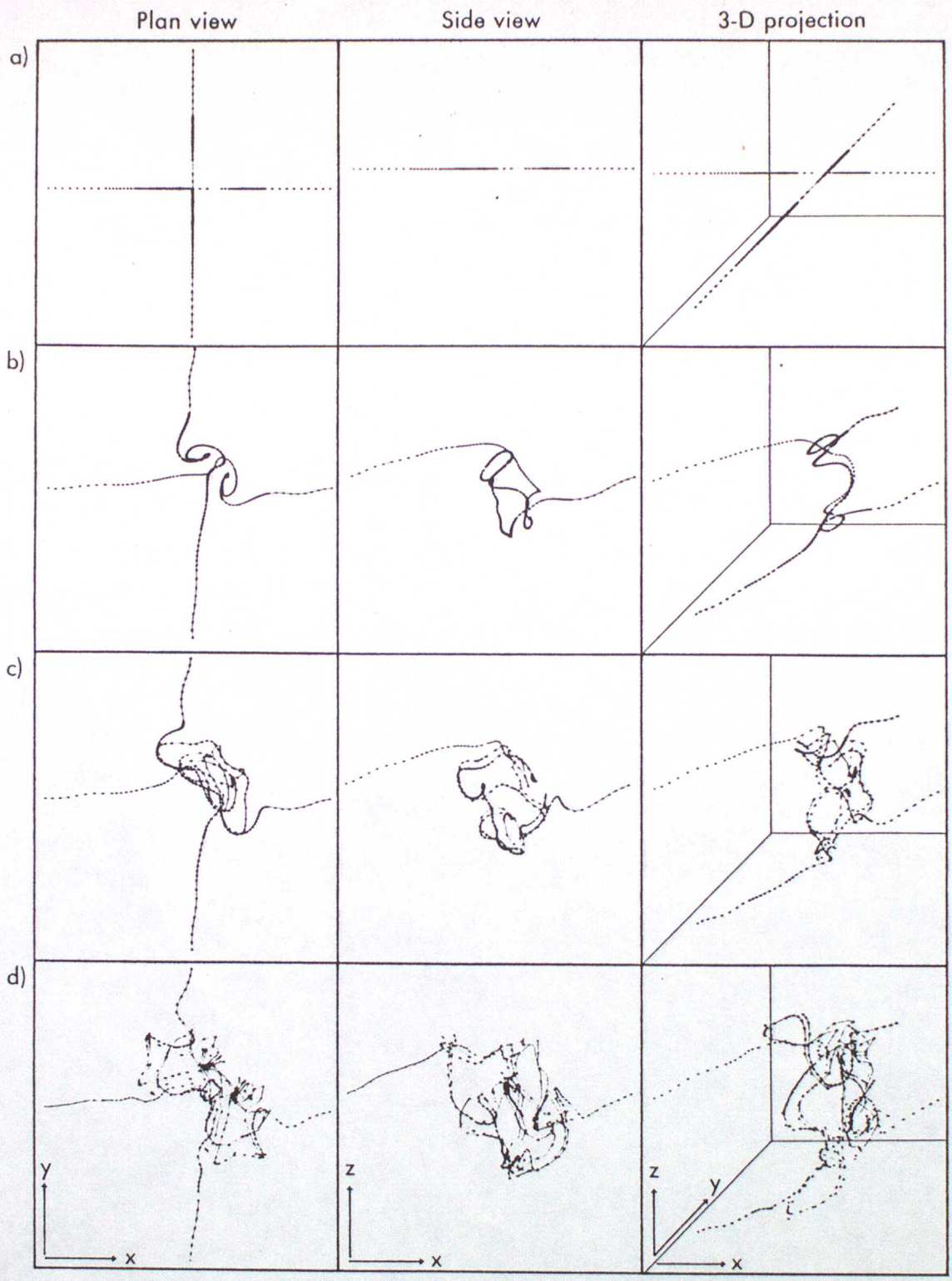

Fig. 1

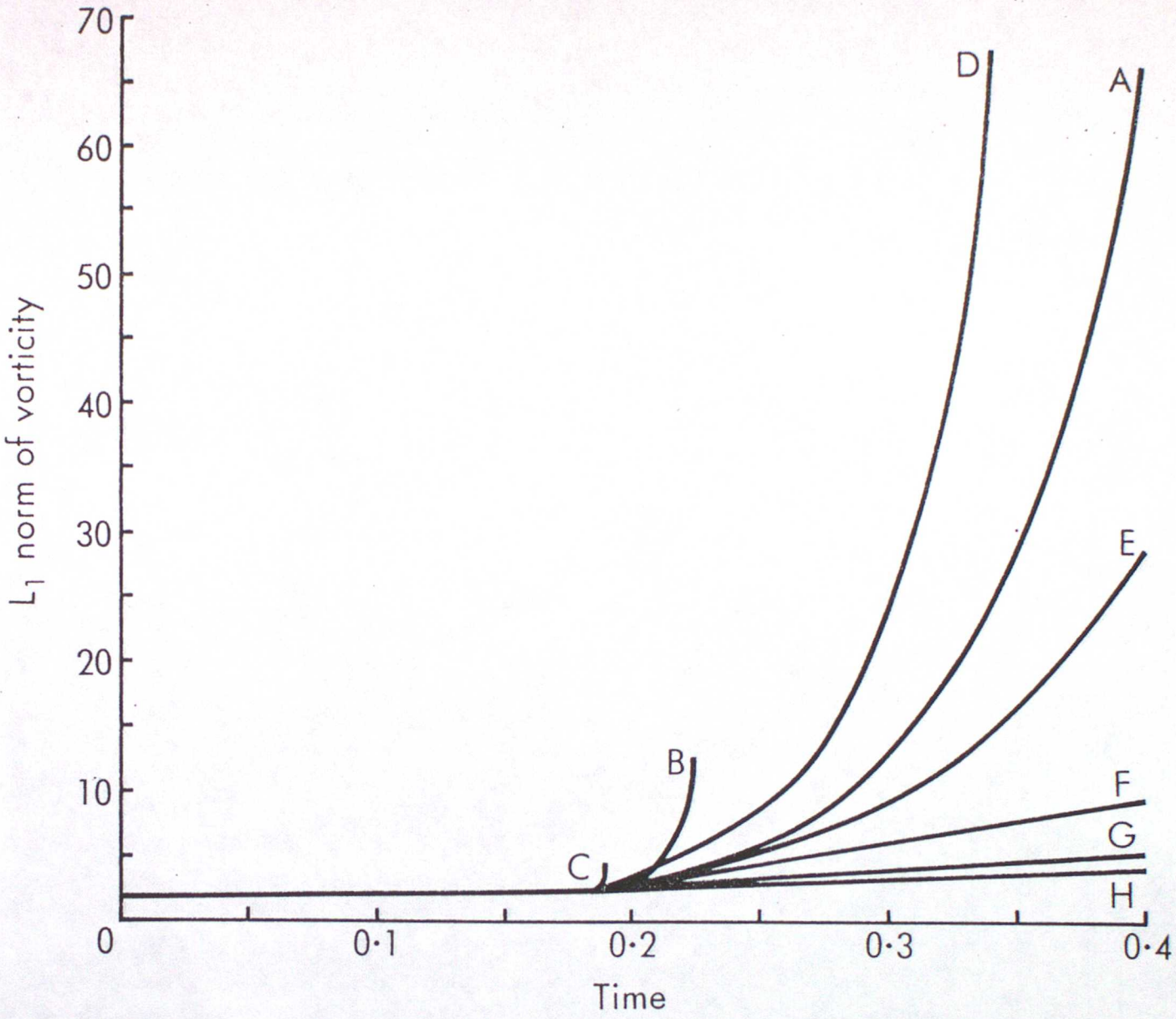
70
60
50
40
30
20
10
0
L_1 norm of vorticity
0·1
0·2
0·3
0·4
Time
A
B
C
D
E
F
G
H

Fig. 2

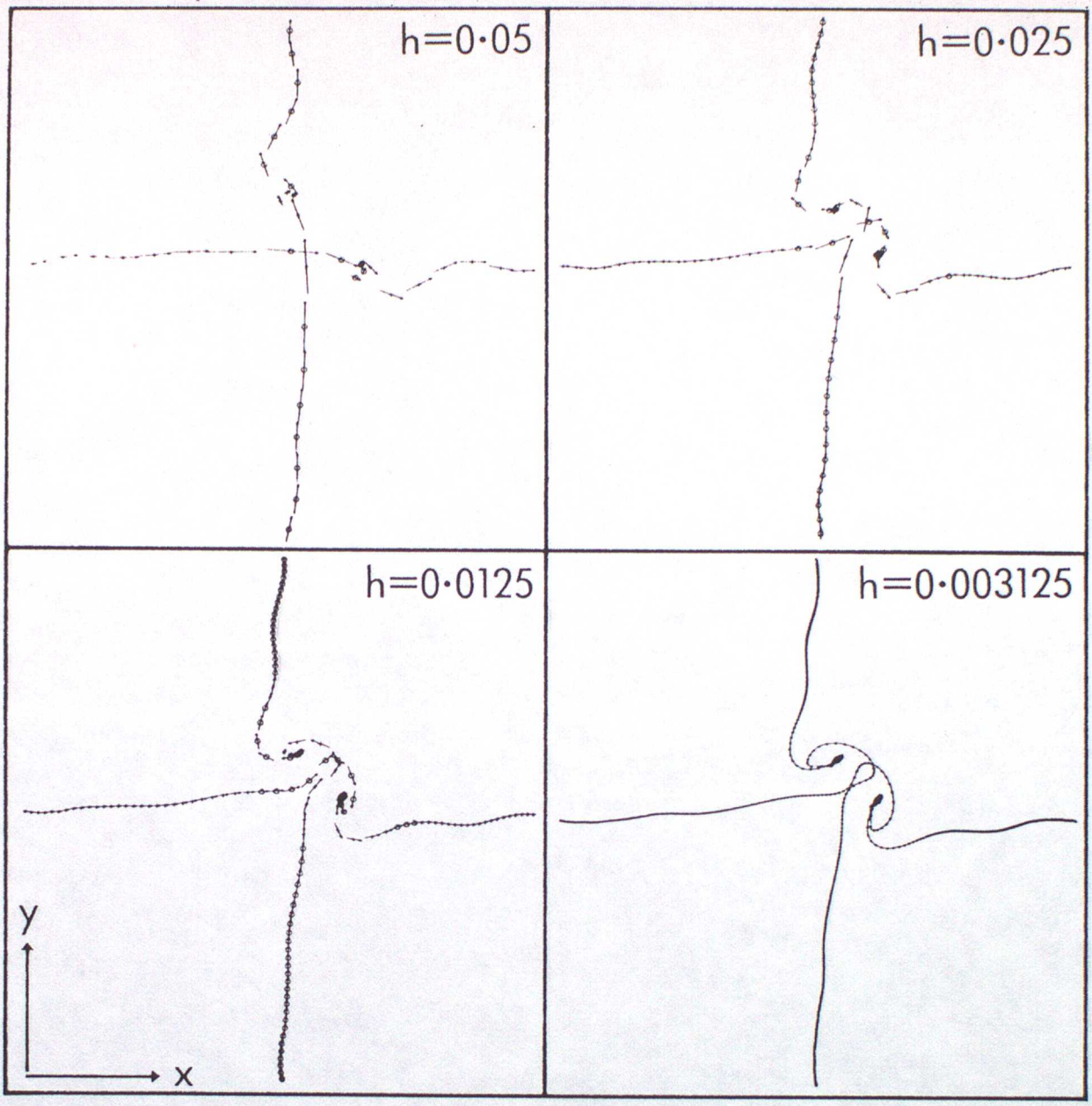

Fig 3.

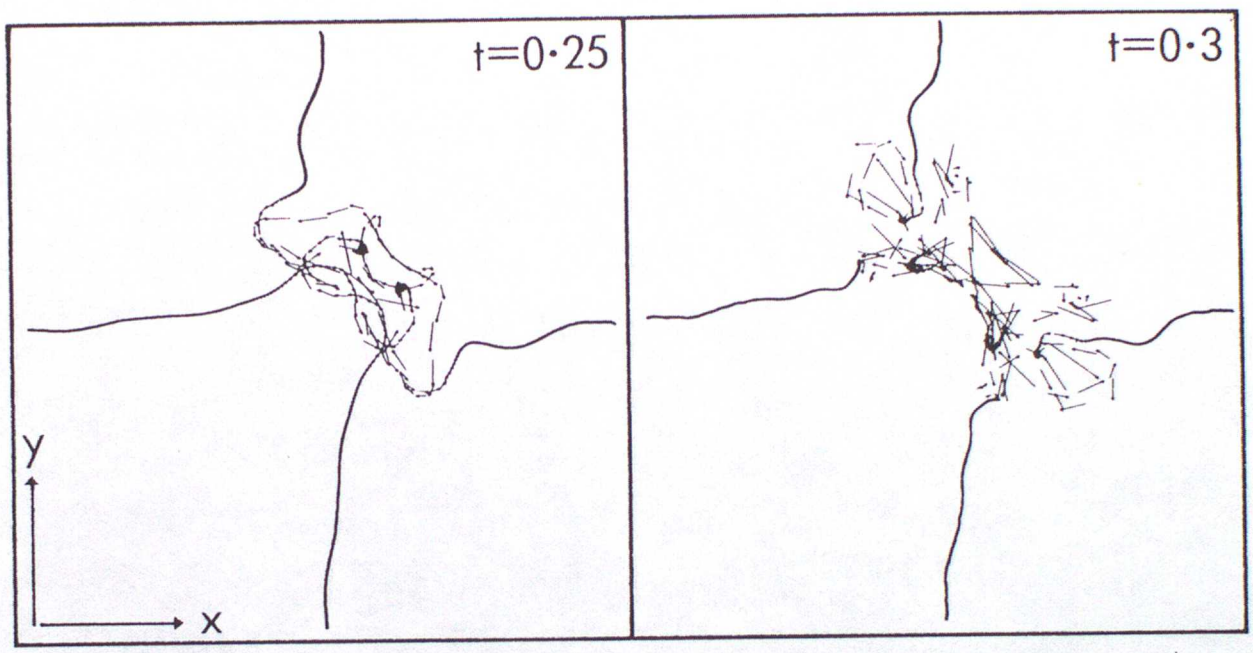

Fig. 4

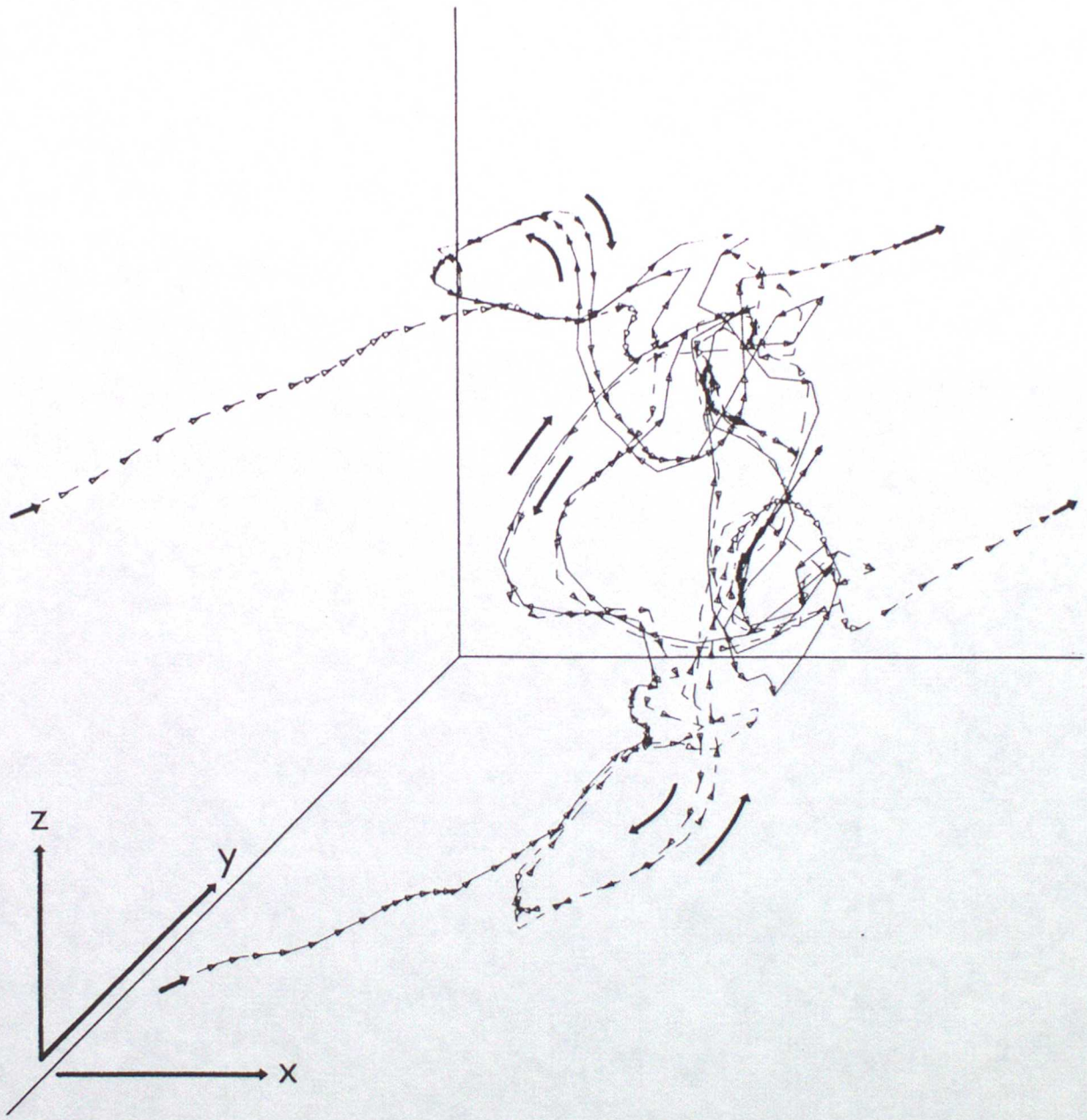

Fig. 5

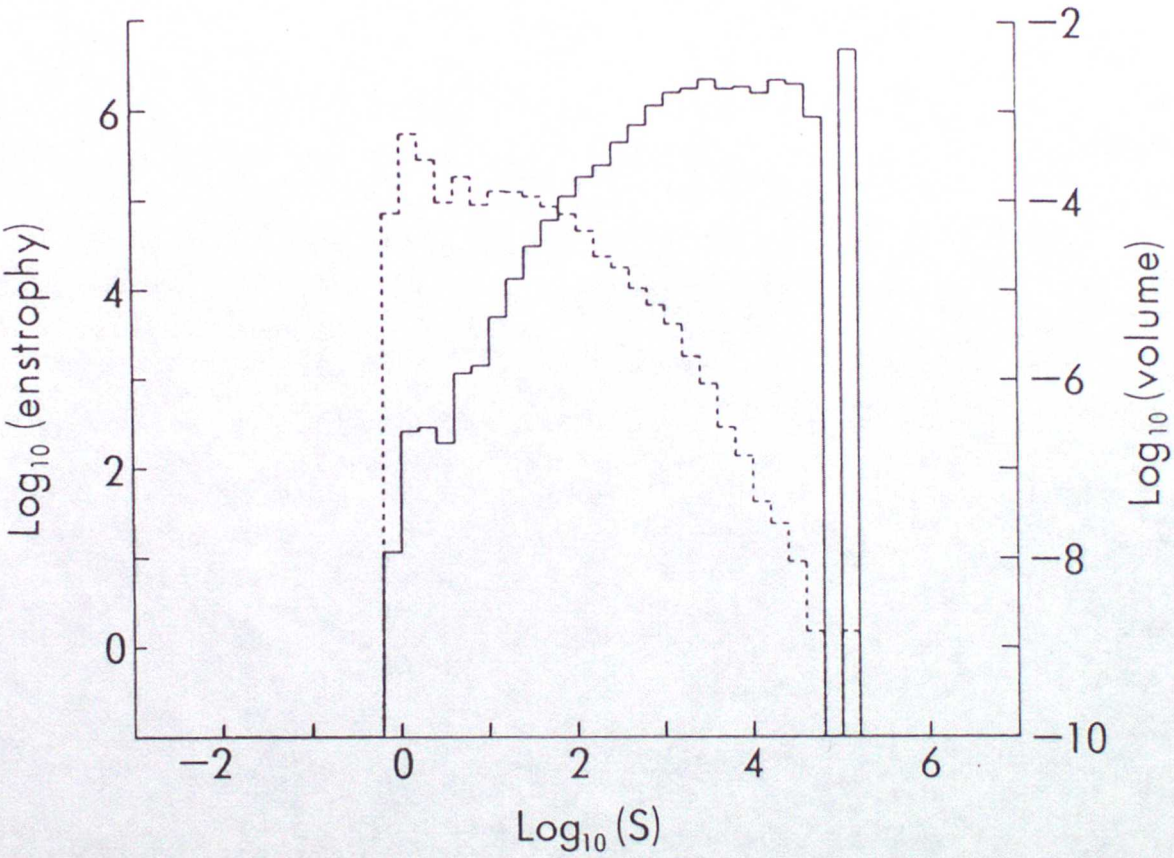

Fig. 6

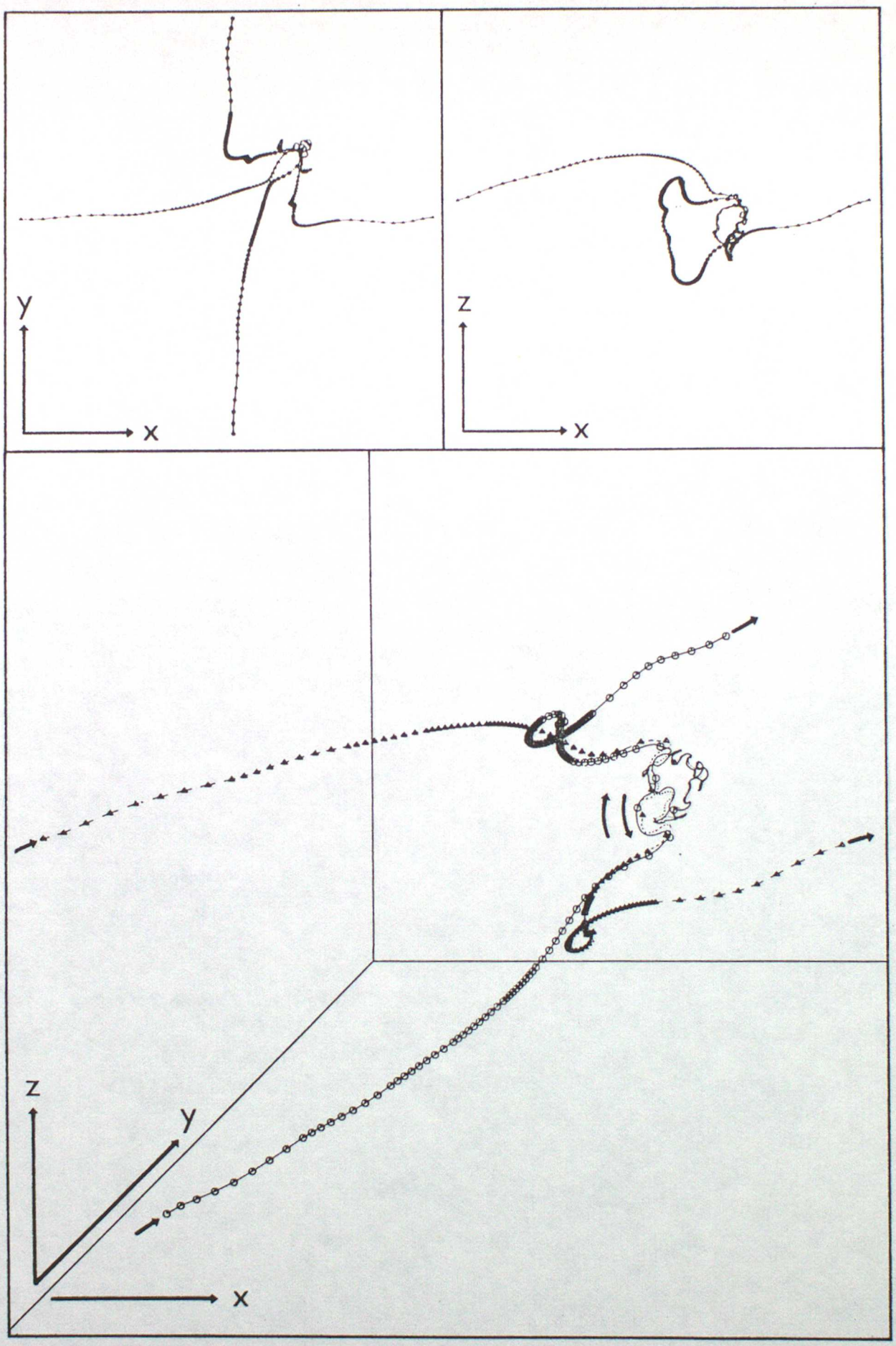

Fig. 7

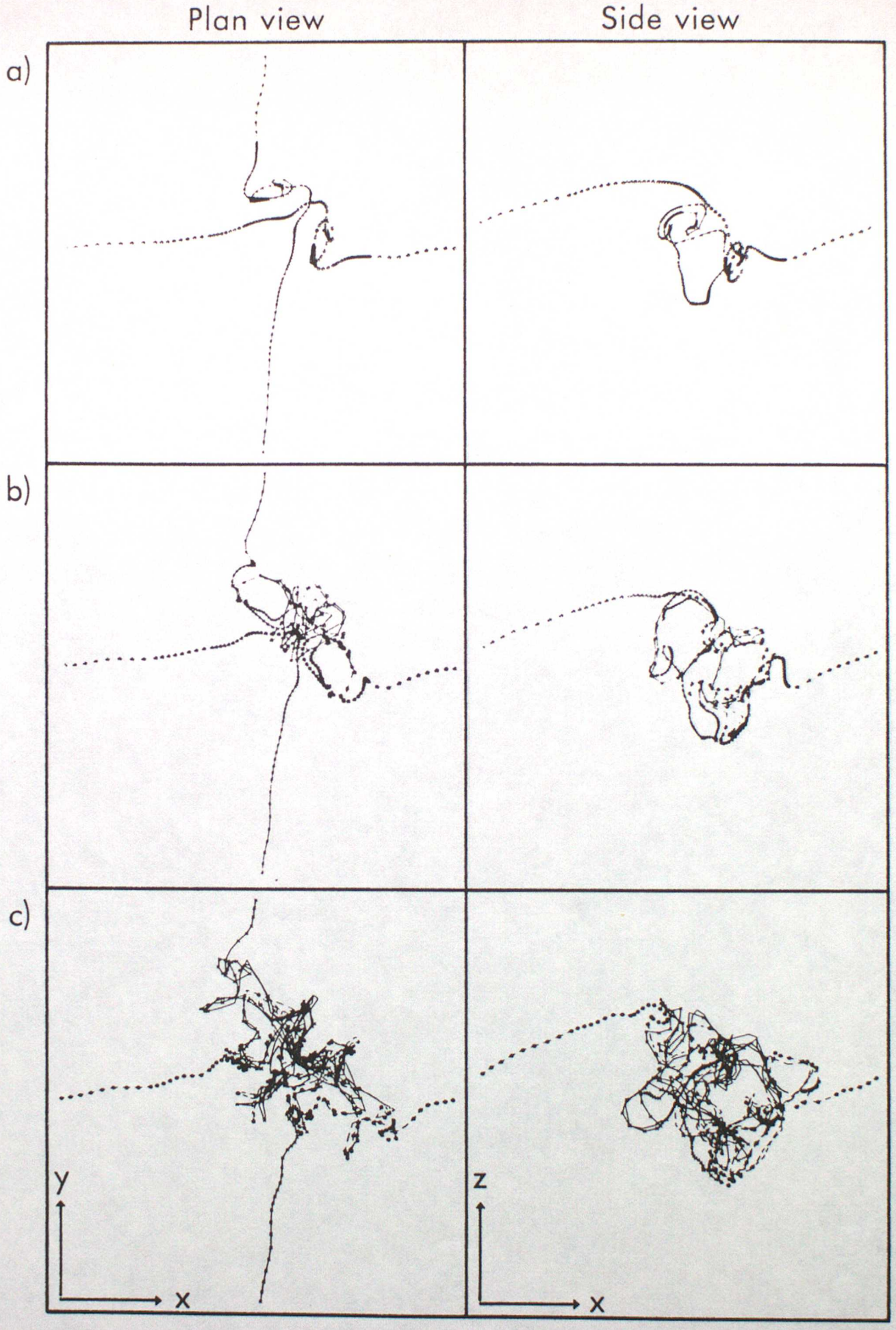

Fig. 8

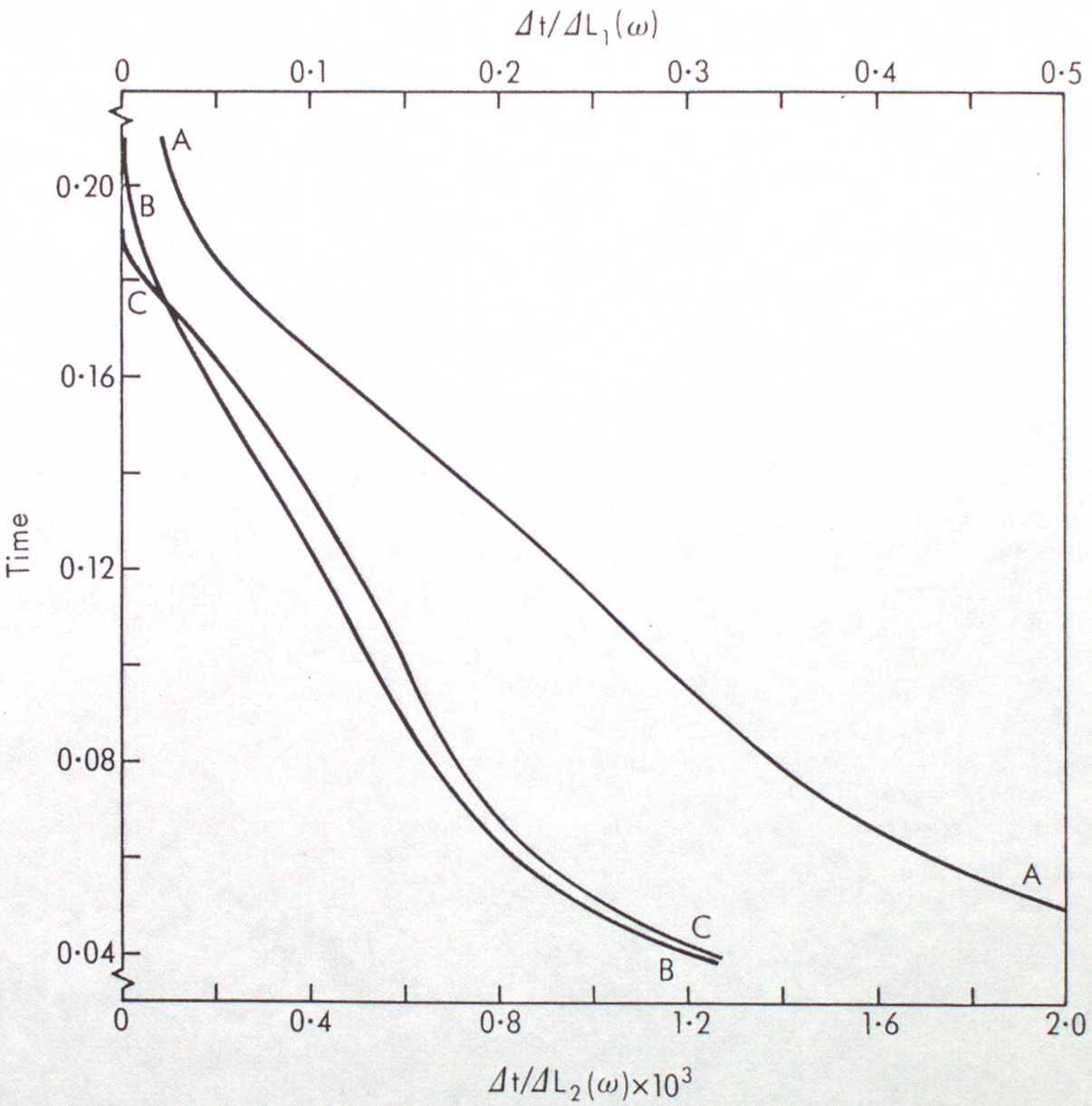
Δt/ΔL1(ω)
0
0·1
0·2
0·3
0·4
0·5
0·20
0·16
0·12
0·08
0·04
Time
A
B
C
A
C
B
0
0·4
0·8
1·2
1·6
2·0
Δt/ΔL2(ω)×10³

Fig. 9